N64-10056

NASA TECHNICAL NOTE

NASA TN D-1979

NASA TN D-1979

EXPERIMENTAL AND THEORETICAL PRESSURES ON BLUNT CYLINDERS FOR EQUILIBRIUM AND NONEQUILIBRIUM AIR AT HYPERSONIC SPEEDS

by Donald M. Kuehn

Ames Research Center

Moffett Field, California

NATIONAL AERONAUTICS AND SPACE ADMINISTRATION • WASHINGTON, D. C. • NOVEMBER 1963

TECHNICAL NOTE D-1979

EXPERIMENTAL AND THEORETICAL PRESSURES ON BLUNT CYLINDERS FOR EQUILIBRIUM AND NONEQUILIBRIUM AIR AT HYPERSONIC SPEEDS

By Donald M. Kuehn

Ames Research Center
Moffett Field, California

NATIONAL AERONAUTICS AND SPACE ADMINISTRATION

NATIONAL AERONAUTICS AND SPACE ADMINISTRATION

TECHNICAL NOTE D-1979

EXPERIMENTAL AND THEORETICAL PRESSURES ON BLUNT CYLINDERS FOR EQUILIBRIUM AND NONEQUILIBRIUM AIR AT HYPERSONIC SPEEDS

By Donald M. Kuehn

SUMMARY

Pressure distributions and shock-standoff distances were obtained in air for three blunt, stream-alined cylinders at a nominal Mach number of 15. Equilibrium stagnation temperature was about 3,600° R, which corresponds to an isentropic exponent in the stagnation region of the model of about 1.25 for the present test conditions. All models were highly cooled. Reynolds numbers based on free-stream properties for equilibrium flow and on cylinder diameter were 2400 and 6200. The experimental data indicated nonequilibrium flow in the stagnation region for some of the models. Viscosity effects appeared to be negligible. Several theories for computing cylinder pressure were examined. Comparisons with experiment showed that some of the existing methods provided good estimates of the pressures on the blunt cylinders. Further evaluation of the theories showed that the blast-wave analogy accurately described the influence of isentropic exponent, as well as Mach number and nose drag, on the cylinder pressure. Perfect-gas characteristics solutions for a wide range of Mach number, nose drag, and isentropic exponent were correlated by the blast-wave parameter and were well represented by a simple, but useful, equation in blast-wave form.

INTRODUCTION

Many methods have been devised for predicting flow fields around blunt vehicles in hypersonic flight so that loads, heat transfer, and vehicle performance can be estimated. The theoretical approaches, which include characteristics solutions, methods based on flow continuity and blast-wave analogy, and Newtonian theory, vary widely in basic formulation and in specific detail. Some of these methods require electronic machine computing; others employ simple equations. Previous investigations indicate that the general character of the flow field can be predicted; however, further comparisons of experiment and theory, especially for real-air flow, are necessary to determine the accuracy and range of application of the theoretical methods. Although limited data are available from shock tunnels for high-temperature air, most evaluations of theoretical surface pressures have been confined to experiments in perfect gases.

Knowledge of surface pressures is important to any study of flow fields about hypersonic vehicles. The present investigation is concerned with this aspect of the flow for blunt, stream-alined cylinders. Study was confined to cylinders of about 10 diameters in length because cylinders of greater fineness ratio are not considered to be of practical significance. Experimental data were obtained for three models in a hypersonic facility in which the vibrational mode of the air molecule was energized to give an equilibrium isentropic exponent in the model stagnation region of about 1.25. Little or no dissociation was present. The purpose of the investigation is to indicate the accuracy with which the various theories estimate the experimental surface pressures on blunt cylinders in air when the isentropic exponent varies over the model, and to investigate the blast-wave correlating parameter by using cylinder pressures from the present experiments and from characteristics solutions.

NOTATION

A^*	nozzle throat area, sq ft
C_D	nose-drag coefficient
D	cylinder diameter, in.
$f(\gamma)$	blast-wave function dependent on γ (See table following eq. (2).)
h	enthalpy, Btu/lb
l	characteristic dimension of the nozzle, $\frac{r^*}{\tan \theta}$, ft
M	Mach number
p	pressure, psia
r^*	nozzle throat radius, ft
R	radius of the spherical noses
$R_{\infty D}$	Reynolds number based on free-stream properties and on cylinder diameter
T	temperature, $^{\circ}R$
U	velocity, ft/sec
W	nozzle mass flow, lb/sec
x	distance along model center line measured from the tip of the nose, in.
x_n	distance along nozzle center line measured from the nozzle throat, in.

x_{n_f} station on nozzle center line at which vibrational freeze is assumed to occur, in.

x_s distance along model center line measured from the nose-cylinder juncture, in.

θ half-angle of conical nozzle, deg

γ isentropic exponent, $\frac{\partial \ln p}{\partial \ln \rho}$ along the local isentrope

ρ density, lb sec^2/ft^4

Δ shock-standoff distance, in.

δ boundary-layer thickness in the model stagnation region, in.

δ^* boundary-layer displacement thickness in the model stagnation region, in.

λ mean free path, in.

τ relaxation time, sec

Subscripts

c corrected for stream gradient

e equilibrium flow

f frozen flow

m measured

n nose of the model

s shoulder at nose-cylinder juncture

stag stagnation region of the model

t total or stagnation conditions

w wall of model

x quantity at station x

∞ free stream

1 ahead of normal shock wave

2 behind normal shock wave

APPARATUS, TEST METHODS, AND DATA REDUCTION

Test Facility

The tests were run in a hypersonic facility with an arc-heated air stream. A nominal Mach number of 15 was attained with a conical nozzle of 15° half-angle and a 6-inch-diameter test chamber. Stagnation enthalpy for these tests, 1000 Btu/lb, was greater than necessary to prevent condensation, but was much less than flight enthalpy at the test Mach number. Stagnation pressures were 380 and 1000 psia. A complete description of the facility is given in reference 1.

Determination of Stream Properties

Properties of the test stream required for reduction and analysis of the experimental pressure distributions were Mach number, pressure, and enthalpy. The flow through the nozzle was assumed to be isentropic. Although the vibrational energy of the nozzle air downstream of the throat was not in equilibrium, calculations of free-stream properties were based upon equilibrium flow. The error is believed negligible, as will be discussed further in subsequent sections. To obtain Mach number from reference 2, pitot pressure was measured in the test chamber, and stagnation values of pressure and enthalpy were determined at tunnel reservoir conditions. Pitot pressure was measured with a Statham transducer; stagnation pressure, with a Bourdon tube gage. Stagnation enthalpy can be obtained from the following empirical equation for the sonic flow of equilibrium air (ref. 3):

$$\frac{W}{A^*} = 19.05\ (h_t)^{-0.4}\ p_t \tag{1}$$

Calculations based on the relaxation time for vibrational equilibrium showed the flow to be in equilibrium up to the throat. The geometric throat area was used in equation (1) since calculations of the boundary-layer thickness indicated that the discharge coefficient at the throat was approximately unity for the highly cooled wall of these tests (i.e., the displacement thickness was approximately zero). Mass flow was obtained with a venturi meter. The pressures at the venturi and within the arc chamber were measured by Bourdon tube gages. The axial distribution of Mach number determined from these measurements is shown in figure 1. Free-stream static pressure was obtained from reference 2 as a function of stagnation pressure, stagnation enthalpy, and Mach number, and values of static pressure and enthalpy were used to obtain the local isentropic exponents from references 4 and 5. It should be noted that references 4 and 5 give slightly different values of γ_{stag} (ref. 4, $\gamma_{stag} \sim 1.22$; ref. 5, $\gamma_{stag} \sim 1.27$). It is not known which is more accurate; however, since only approximate values are of interest here, a value of 1.25 was used.

Models

The models were blunt, stream-alined cylinders. The three nose shapes investigated had considerably different drag coefficients (fig. 2). All models were machined from stainless steel and had a cylinder diameter of 0.625 inch. Orifices were located at only two longitudinal stations on the basic cylindrical section because of space restrictions due to the size of pressure tubing dictated by requirements of response time. To minimize response time, surface pressure at each station was measured with eight 1/16-inch diameter orifices equally spaced around the cylinder circumference. To obtain data at various longitudinal locations cylindrical extensions of different length were inserted between the basic cylinder and the nose section, thus moving the orifice stations farther from the tip of the nose. The location of the nose was maintained at the same tunnel station for all cylindrical extensions.

Transducers for Surface-Pressure Measurement

Model-surface pressure was measured with two types of pressure transducers, a Statham transducer and a vibrating diaphragm transducer (ref. 1). Both types, located outside the test chamber, were connected in parallel to measure the pressure simultaneously at each of the two model stations. The Statham transducer is a commercially available strain-gage type. The vibrating-diaphragm transducer relates the energy required for driving an oscillating diaphragm, at fixed amplitude, to the pressure of the gas within the transducer. The vibrating-diaphragm transducer has a number of theoretical advantages over the Statham transducer, but both systems were used because the dependability of the vibrating-diaphragm system had not been established. The output of the transducers was measured with an Offner recorder. Typical pressure traces reproduced in figure 3 show negligible change during the last half of the 4 second run, indicating that the pressures attained equilibrium. The pressures were obtained by measuring the deflection of the trace from a zero reference and applying a calibration constant. Results from the two transducers agreed with each other within the accuracy that a given transducer could repeat a measurement from run to run.

Flow Visualization

The flow field around the blunt cylinders was observed by use of the glow-discharge technique described in reference 1. Briefly, the system operates on the principle that ionized air produces a visible glow. A high-voltage potential between an anode mounted in the tunnel wall and the model ionizes the air around the model. The intensity of the glow is proportional to the number of ionized particles, and the number of particles is proportional to the air density. Photographs of the glow, shown in figure 4, reveal the bow shock wave.

Correction for Free-Stream Gradient

Pressures on the blunt cylinders were affected by the gradient in the free stream. Corrections were, therefore, added to the measured pressures to obtain a pressure distribution approximately equivalent to that which would have been measured in a stream with no gradient. A correction commonly used for such data is equal to the difference between the free-stream static pressures at the nose of the model and at a particular body station. This correction for the present investigation is shown in figure 5. Application of such a correction is, of course, subject to the uncertainty involved in the linear superposition of two pressure gradients. Both the measured pressures and the corrected pressure distributions will be presented later.

RESULTS AND DISCUSSION

Theories for Determining Cylinder Pressures

Several theoretical methods will be considered to determine how well the predictions agree with experimental pressures on the surface of blunt, stream-alined cylinders. The theories to be evaluated are the unmodified blast-wave theory (ref. 6), perfect-gas characteristics solutions[1] (refs. 7 through 10 and unpublished solutions by the method described in ref. 10), a real-air characteristics solution by Inouye and Lomax, Ames Research Center (this method is an extension of the method described in ref. 10), a flow-continuity method (ref. 11), and a pressure-decay method (modified blast-wave theory, ref. 12). These methods will be discussed before comparisons with experiment are made.

Blast-wave theory.- Surface pressures on blunt cylinders can be estimated by a theory based on an analogy between the development of a cylindrical blast wave and the hypersonic flow about a slender, stream-alined cylinder. This blast-wave theory is presented in reference 6 as a first-order approximation which includes a function of γ,

$$\frac{p_x}{p_\infty} = f(\gamma)\,\frac{M_\infty{}^2 C_D{}^{1/2}}{x/D} \tag{2}$$

[1]The method of characteristics applied to the flow over a blunt body requires a previous calculation of the subsonic portion of the flow, and proper matching of the subsonic and supersonic regions. For simplicity of expression this total computation procedure will be referred to as a characteristics solution.

where $f(\gamma) = 1/8\ (\gamma/J_o)^{1/2}\ g(\delta)$ has the following values (refs. 6 and 13, and calculations made at Ames Research Center)

γ	$f(\gamma)$
1.2	0.052
1.3	.061
1.4	.067
1.67	.084

A second-order approximation for $\gamma = 1.4$ (ref. 6) is

$$\frac{p_x}{p_\infty} = 0.067\ \frac{M_\infty{}^2 C_D{}^{1/2}}{x/D} + 0.44 \tag{3}$$

Additional functions necessary to the solution of the second-order approximation for values of γ other than 1.4 have not been computed. A blast-wave equation in second-order form which describes γ effects can, however, be obtained by applying the first-order γ effect (eq. (2)) to the second-order solution for $\gamma = 1.4$ (eq. (3)), noting that $f(\gamma) = 0.067$ for $\gamma = 1.4$. The following equation results:

$$\frac{p_x}{p_\infty} = \frac{f(\gamma) M_\infty{}^2 C_D{}^{1/2}}{x/D} + 0.44 \tag{4}$$

This equation might be expected to be more useful than equation (2) or (3)

Perfect-gas characteristics theory.- Surface pressures on blunt cylinders computed by the perfect-gas characteristics method can be correlated to avoid the necessity of additional characteristics solutions for each new combination of M_∞, C_D, and γ for which the distribution of cylinder pressure is desired. Pressures from characteristics solutions for a wide variety of Mach numbers and nose shapes were correlated for each of two perfect gases in reference 7 using the parameter $(M_\infty{}^2 C_D{}^{1/2})/(x/D)$. Good correlations were obtained for each gas, except close to the nose. Equations which describe the correlated pressures for $p_x/p_\infty > 1$ are as follows (ref. 7):

$$\frac{p_x}{p_\infty} = 0.060\ \frac{M_\infty{}^2 C_D{}^{1/2}}{x/D} + 0.55\ , \qquad \gamma = 1.40 \tag{5}$$

$$\frac{p_x}{p_\infty} = 0.075\ \frac{M_\infty{}^2 C_D{}^{1/2}}{x/D} + 0.55\ , \qquad \gamma = 1.67 \tag{6}$$

Equations (5) and (6) reduce to the following equation if the γ influence described by equation (2) is considered (ref. 14):

$$\frac{p_x}{p_\infty} = 0.89 \frac{f(\gamma)M_\infty{}^2 C_D{}^{1/2}}{x/D} + 0.55 \tag{7}$$

Perfect-gas solutions for blunt cylinders by Edsall (ref. 8), Vaglio-Laurin and Trella (ref. 9), and by Inouye and Lomax (ref. 10 and unpublished solutions) have also been used to test this correlation further. Pressures close to the nose have been excluded in accord with a criterion to be described. Figure 6 shows that these solutions are slightly below the curve described by equation (7). The difference cannot be attributed to the fact that the Van Hise data are all for sharp noses because a sonic-cone solution by Inouye and Lomax at $M_\infty = 14.4$ agrees with the blunt-body solutions. The reason for the difference is not known, but it is possible that different programming methods could cause slight differences in characteristics solutions. All data in figure 6 are represented by the following equation which describes the computed pressures within about 5 percent for p_x/p_∞ greater than 0.9 (except for small values of x/D):

$$\frac{p_x}{p_\infty} = 0.85 \frac{f(\gamma)M_\infty{}^2 C_D{}^{1/2}}{x/D} + 0.55 \tag{8}$$

There is little doubt that the perfect-gas blast-wave parameter provides an excellent correlation of a wide variety of perfect-gas characteristics solutions. Equation (8) will be used to represent perfect-gas characteristics solutions in subsequent comparisons of theory and experiment.

Pressures obtained by the characteristics solutions are below the blast-wave correlation for small values of x/D (ref. 7). This deviation occurs because a distance of several body diameters is required to relieve the infinite overprediction of pressure by blast-wave theory at the stagnation point. Lukasiewicz (ref. 6) examined the solutions of reference 7 to obtain curves representing the minimum x/D for correlation as a function of M_∞ and C_D for $\gamma = 1.40$. The solutions of reference 7 for $\gamma = 1.40$, as well as for $\gamma = 1.67$, have been re-examined in the present investigation. The results, along with additional data from the characteristics solutions by Inouye and Lomax, are plotted in figure 7(a) as a function of C_D and γ. A definite trend with γ was observed, thus the minimum x/D for correlation was adjusted by the γ function as shown in figure 7(b). Apparently the value of $(x/D)_{min}$ is not dependent on Mach number. This limitation, imposed on the correlation of characteristics solutions in figure 6, applies to equation (8).

Real-air characteristics theory.- The method of characteristics for real air should, by virtue of basic formulation, predict the experimental flow very accurately if viscous effects are small. Several real-air characteristics methods have been programed (e.g., see refs. 8 and 9); however, collection and correlation of real-air solutions have not progressed sufficiently to present an analysis parallel to that for the perfect-gas solutions. A solution by Inouye

and Lomax was, however, obtained for the equilibrium flow of real air over a hemisphere cylinder with a sonic starting cone for the specific test conditions of the present experiments (extension of the program to blunt bodies and shapes with slope discontinuities is not yet completed). This solution will be compared later with experiment.

Flow-continuity method.- Flow fields around blunt bodies can also be computed by utilizing the principle of conservation of mass flow. A method based on this concept (ref. 11) equates the mass flow of real air through the shock wave with that at a particular body station. The flow field is divided into many stream tubes for which mass-flow calculations are made. The shape of the bow shock must be known, and the static pressure distribution between body and shock is assumed to have the same form as that given by first-order blast-wave theory. Experimental shock-wave shapes were used in the present calculations. This method gives the flow-field properties at any desired longitudinal station without knowledge of flow properties at other intermediate stations. This, of course, is a worksaving advantage over methods which require a numerical buildup of the entire flow which precedes the station at which flow properties are desired. The flow-continuity method has been programed for electronic machine computing.

Pressure-decay method.- The pressure distribution on a blunt cylinder can be determined by considering the rate at which the pressure decays from some initial value, as described by blast-wave theory. An equation for the cylinder pressure, based upon the pressure decay of a blast wave with cylindrical symmetry, is as follows (ref. 12):

$$\frac{p_x}{p_\infty} = \frac{1}{1 + (x_s/D)} \frac{p_s}{p_\infty} + \left\{\frac{1}{1 + [1/(x_s/D)]}\right\}^{p_s/p_\infty} \tag{9}$$

In other investigations (refs. 15 and 16) the pressure-decay equation has been modified to make use of experimental values of pressure at the shoulder and far downstream. Such empirical modifications should reveal how well the equation will predict the rate of pressure decay, but these alterations are not justified if the equation is to be used for the prediction of pressures. The present evaluation of equation (9) allows p_x/p_∞ to approach 1 as x_s/D approaches infinity; however, satisfactory values of shoulder pressure are not conveniently available for the geometries and test conditions of the present investigation. Reference 12 gives shoulder pressure as a function of Mach number for hemisphere-cylinders for $\gamma = 1.4$, and reference 8 does similarly but without consideration of γ. The value of shoulder pressure used in the present calculation for the hemisphere-cylinder was obtained from reference 12 ($p_s/p_{t_2} = 0.045$ for $M_\infty = 14.4$). Although the pressure-decay method is intended primarily for rounded blunting, calculations were also made for the flat-faced cylinder and the blunt cone cylinder. Shoulder pressures are not available for these configurations at the desired values of γ. A very crude, but simple, approximation of the initial pressure from which the decay process begins for these models was obtained by adjusting the value for the hemisphere-cylinder in proportion to $C_D^{1/2}$, as indicated by blast-wave theory, without regard to nose length. Obviously, the subsequent comparisons of pressure distributions by the pressure-decay method with

experiment will be of qualitative interest only because the quantitative agreement is determined entirely by this rather questionable choice of shoulder pressure.

Experimental Data

Cylinder pressure distributions.- The measured pressures, normalized by free-stream pressure at the model nose, are shown in figure 8 in terms of the longitudinal distance x/D. The points represent repeat runs as well as the duplicate data obtained by the two different sets of pressure cells. The scatter of the data points is, therefore, a good representation of the error of measurement. The pressure distributions corrected for center-line, free-stream Mach number gradient are shown in figure 8 by the dashed lines. Only these corrected pressure distributions will be used in the data analysis.

Effects of viscosity.- Analysis of the experimental data must include an estimate of the effects of viscosity, because such effects will, of course, limit comparisons between experiment and inviscid theory. The influence of viscosity for the present tests on both the shock-standoff distance and on the cylinder pressure will be discussed.

The shock-standoff distance, Δ, can be influenced by viscosity at low Reynolds numbers. Since Δ depends on mass flow, the value of Δ for viscous flow will differ from the value for inviscid flow by approximately δ^*. The value of δ^*/Δ_e is estimated to be 0.06 for the spherical-tipped cone and 0.04 for the hemisphere-cylinder, so that the displacement-thickness correction is not significant. The extremely small δ^* for these models was due to the large amount of wall cooling ($T_w/T_t \sim 0.15$). An additional effect of viscosity on the shock-standoff distance, discussed in the theoretical analyses of references 17 and 18, is that for sufficiently low Reynolds numbers the vorticity modifies the shock layer so that the boundary-layer concepts must be modified. Six flow regimes were described in reference 17, but only those significant to the classification of the present experiment will be mentioned. The first is the vorticity interaction regime, characterized by a thin shock, an inviscid layer, and a boundary layer. As the Reynolds number is reduced, the viscous-layer flow regime is approached. The entire shock layer becomes viscous, but the shock remains thin. Reducing the Reynolds number further causes the viscous layer to merge with a thickened shock wave (merged-layer flow regime). Reference 17 indicates that the boundaries between these flow regimes are as follows: vorticity interaction regime, $\lambda_\infty/R \ll \rho_1/\rho_2$; viscous layer regime, $\lambda_\infty/R \ll (\rho_1/\rho_2)^{1/2}$; incipient merged layer regime, $\lambda_\infty/R \ll 1$. The value of λ_∞ for the present calculations was computed by the method of reference 19, in which the air molecule was considered to be elastic. The value of λ_∞/R for the model with the smallest nose radius is 0.03. The value of ρ_1/ρ_2 for equilibrium flow is 0.147. It appears that for this model the test conditions were close to the borderline between the vorticity interaction and the viscous layer regimes. A similar classification of the present experimental conditions is determined from figure 4 of reference 20. This classification is also consistent with the present boundary-layer calculations which gave $\delta^* \sim 0.001$ inch and $\delta/\delta^* \sim 15$. Reference 17 showed that the shock-standoff distance for a sphere in the viscous layer regime is larger than

the inviscid value. This analysis was for incompressible flow in the stagnation region (constant density). Reference 18 removed the constant density restriction, with the result that the standoff distance was less than the inviscid value over the valid range of the theory. These two results are contradictory, but the analysis of reference 18 is probably more accurate because compressible flow was considered. The present experimental data will be analyzed assuming, as shown in reference 18, that viscosity does not cause the shock-standoff distance to be greater than the inviscid value.

In contrast to the viscous effects shown in reference 15, viscosity does not appear to have a significant influence on the cylinder pressures for the present investigation. Good agreement of the data shown in figure 9 for two values of Reynolds number indicates that viscous effects were not measurable in the present tests. (Maximum scatter of these data is about 10 percent.) Although this Reynolds number variation is small, a comparable variation in reference 15 produced a 15- to 20-percent change in cylinder pressure. Further, the expected change in cylinder pressure for the present data, based on information in reference 15, should be much greater than 15 to 20 percent because of the lower Reynolds number of the present data. A fundamental difference between these two experiments is the degree of wall cooling. The data of reference 15 represent an adiabatic wall and the present data are for a highly cooled wall ($T_w/T_t \sim 0.15$). Wall cooling decreases the boundary-layer displacement thickness, thus variations in Reynolds number might be less significant. For the present tests, boundary-layer calculations show the displacement thickness at the stagnation point to be very small ($\delta^*/R \sim 0.006$). Since no Reynolds number effect is indicated in the present data, only the higher Reynolds number data will be used subsequently.

Degree of flow equilibration.- The degree of flow equilibration must be estimated in order to interpret the present experimental data. Calculations of relaxation times, mean free path and molecular velocity in the model stagnation region, shock-standoff distances, and pressure distributions were considered in this evaluation. These calculations indicate that the vibrational energy mode of the air in the nozzle free stream was not in equilibrium. The calculations and test results further indicate that the flow in the shock layer for some of the experimental models was not in vibrational equilibrium and possibly not in rotational equilibrium. These results will be presented.

Nonequilibrium flow in a nozzle alters the properties of the test stream from those associated with equilibrium flow. If the present tests were under equilibrium conditions, the isentropic exponent in the nozzle would vary from about 1.29 at the throat to 1.40 at an x_n of 0.8 inch. Correspondingly, the vibrational energy mode of the air would be inactive for values of x_n greater than 0.8. The possible occurrence of vibrational nonequilibrium is, therefore, of concern for values of x_n less than 0.8. To examine the nozzle flow for nonequilibrium conditions, values of relaxation time for nitrogen and oxygen from reference 21 were used to obtain the relaxation distance along the nozzle center line, τU_e, in terms of a reference length, l (fig. 10). Interpretation of these calculations to delimit the equilibrium, nonequilibrium, and frozen flow regimes is approximate. From these calculations it appears reasonable to conclude, however, that the flow was in equilibrium up to the throat and probably nonequilibrium for a few tenths of an inch downstream of the throat, where the oxygen and nitrogen were relaxing at different rates. This would be followed by

frozen flow. The concept of equilibrium flow followed by sudden vibrational freeze may not be realistic, but it does provide a convenient means for estimating the influence of nonequilibrium nozzle flow on the free-stream properties. Figure 11 illustrates the rapid approach toward equilibrium for Mach number in the test region for various locations of vibrational freeze. This return to equilibrium is, of course, consistent with the variation of equilibrium isentropic exponent in the nozzle which was mentioned earlier. Other stream properties also return to equilibrium as x_{n_f} approaches 0.8. It is obvious from figure 11 that equilibrium flow for a very short distance downstream of the throat will result in near-equilibrium free-stream properties. It appears from figure 10 that vibrational freeze at the throat would be slightly conservative. More likely, the values of stream properties are between those for freeze at the throat and equilibrium, and thus are not far from the equilibrium values. Equilibrium stream properties will be used in subsequent calculations and the resulting error will be estimated.

Flow equilibration in the shock layer can be estimated theoretically from the number of molecular collisions necessary for equilibrium between the various energy modes. Based upon equilibrium flow properties, the time for 1 molecular collision can be computed for the model stagnation region (ref. 19). The resident time from shock wave to body can be estimated from the value of Δ_e and the shock layer velocity (values of Δ_e were determined from refs. 22 and 23). A molecule will have about 230 collisions in the stagnation region for the blunt cone, about 460 for the hemisphere-cylinder, and about 1900 for the flat-faced cylinder (the values which correspond to the condition of vibration frozen at the nozzle throat and equilibrium in the shock layer are not significantly different from those quoted). The number of molecular collisions required for equilibration of air is rather nebulous, however, estimates are generally in agreement that translational equilibrium requires only a few collisions. The number of collisions for rotational equilibrium appears to be in the range of 10 to 100. Estimates regarding the number of collisions for vibrational equilibrium range from a few hundred to many thousand. It is clear that the flow was in translational equilibrium for all the present models. Rotation was possibly nonequilibrium for a significant portion of the shock layer for the blunt cone, close to equilibrium for most of the shock layer for the hemisphere, and essentially in equilibrium for the flat-faced cylinder. Vibration was probably nonequilibrium for the blunt cone and for the hemisphere, but the degree of vibrational relaxation for the flat-faced cylinder is not apparent.

Measured shock-standoff distances provide experimental information on the state of the flow in the model stagnation region. The standoff distance for inviscid nonequilibrium flow in the shock layer will be larger than that for equilibrium flow. Observed increases in Δ_m over the equilibrium value will, therefore, be interpreted as indicative of nonequilibrium flow because it has been shown previously that viscous effects will not increase Δ measurably for the present data. Theoretical values of Δ/Δ_e for equilibrium in the stagnation region ($\gamma_{stag} \sim 1.25$), vibration frozen at the free-stream condition ($\gamma_{stag} = 1.4$), and both vibration and rotation frozen at the free-stream condition ($\gamma_{stag} = 1.67$) are 1, 1.2, and 2.0, respectively. The values of Δ/Δ_e corresponding to those flow conditions in the model stagnation region for vibration frozen in the nozzle at the throat are 1.1, 1.2, and 2.0, respectively.

Obviously, the measured shock-standoff distance cannot be used to deduce whether the nozzle flow was in vibrational equilibrium because the data are not sufficiently accurate to detect the small change in Δ due to free-stream nonequilibrium. On the other hand, the analysis of the flow in the model stagnation region using standoff distances was not impaired by the state of the free stream because Δ was not significantly affected. The theoretical values of Δ/Δ_e for nozzle flow in equilibrium are shown in figure 12 with experimental values of shock-standoff distance (data for other models are shown also to establish the trend more firmly). Interpretation of this comparison of experimental and theoretical shock-standoff distances with regard to the degree of flow equilibration in the model stagnation region is consistent with the analysis based upon the number of molecular collisions. In addition, the present experiment indicates that vibrational equilibrium is probably attained for the flat-faced cylinder, whereas the analysis based on molecular collisions was not conclusive regarding this point. It should be mentioned, however, that the state of vibrational equilibration for the flat-faced cylinder deduced from present shock-standoff distances is different from that which would be obtained using Blackman's relaxation times. Blackman's data applied to the present test conditions would indicate that vibration was frozen at the free-stream conditions throughout the stagnation region for all the models. This conflict cannot be settled with the information at hand. The chosen values of γ_{stag}, which are used in subsequent data analysis, are consistent with the present experiment. These values[2] are ~1.25 for the flat-faced cylinder, ~1.4 for the hemisphere-cylinder, and ~1.5 for the spherical-tipped cone. The occurrence of nonequilibrium flow in the nozzle will not alter these values.

Pressures on a blunt cylinder can also provide a measure of the isentropic exponent of the flow if the perfect-gas blast-wave theory can be applied. Equation (2) describes the dependence of pressure on γ according to blast-wave theory. When the isentropic exponent varies within the flow field (real-air flow), the value of γ in the model stagnation region might be considered significant (ref. 14). A variation of the isentropic exponent in the stagnation region caused by a variation in the degree of flow equilibration could, then, be expected to change the surface pressures. The comparison of experiment and theory in figure 13 indicates a probable variation of γ for the experimental data for the three models; namely, the bluntest model had the smallest value of stagnation γ. This variation is consistent with that deduced from previous analyses. Further, if the information in figure 13 is considered quantitatively, deduced values of γ_{stag} would be very close to those obtained from the analysis of shock-standoff distances.

---

[2]These values of γ_{stag} are slightly different from those quoted in reference 14. The value for equilibrium flow was revised to represent a better average of references 4 and 5. The nonequilibrium values were revised upward in view of the indicated rotational nonequilibrium and the absence of significant viscous effects. Since the trend of γ_{stag} with model size is much more important than actual magnitude, this revision does not alter the conclusions of reference 14 nor does it measurably affect the correlations.

Evaluation of the Theories

The theoretical methods discussed previously will be evaluated by comparisons with experiment. Blast-wave theory will be used to correlate the present experimental pressure distributions in a form that will be most convenient for subsequent comparisons with theoretical predictions. Previous discussion poses a question, however, with respect to the influence of nonequilibrium nozzle flow on these comparisons of experiment and theory. Prior to these comparisons, therefore, it will be necessary to assess the influence of an error in the nozzle flow properties on the correlated experimental pressure distributions.

Blast-wave correlations.- The blast-wave correlating parameter is intended for perfect gases, but the possible extension of this perfect-gas theory to real air will be examined. It is not clear, however, whether a single value of γ will characterize a particular flow field in which γ actually varies. It was suggested in reference 14 that the value of γ in the stagnation region might be the significant one. The present experimental data provide an opportunity to apply the blast-wave theory to real-air flow because the value of γ in the model stagnation region is different for each of the three nose shapes (see discussion of nonequilibrium flow) and in addition the value of γ varies within the flow field. These data, shown in figure 14(a), are not correlated by the parameter which does not consider γ (eq. (3)). The improved correlation shown in figure 14(b) indicates that the stagnation γ might well be the significant quantity, in spite of the recognized variation in γ along the body for real-air flow. (This correlation of experiment is not affected by nonequilibrium nozzle flow because any error in M_∞ and p_∞ will apply to each pressure distribution.) Further, the correlation adds strength to the conclusion that the experimental stagnation γ was different for each model and is in the direction previously deduced, and also indicates that the values of γ are approximately as specified.

Influence of nonequilibrium nozzle flow on correlated pressures.- Before proceeding to the comparisons of experiment and theory, it was necessary to examine the influence of nonequilibrium nozzle flow on the correlated pressure distributions. The free-stream properties of concern were Mach number and static pressure. At worst (vibrational freeze at the nozzle throat) the value of M_∞ would be 15.5; thus the correlated experimental pressures (fig. 14(b)) would be shifted to the left by $(14.4/15.5)^2 = 0.863$. The corresponding upward displacement due to the difference in p_∞ is 1.18. The pressure distribution for the blunt cone-cylinder model is shown in figure 15 referred to free-stream conditions both for equilibrium nozzle flow and for vibrational freeze at the throat. The experimental data for the other two models will shift correspondingly. Although the shift in individual data points is significant, the resulting pressure distribution curve is not significantly different from that for which equilibrium conditions of M_∞ and p_∞ were used. Further, it is not expected that the flow was frozen at the throat, as discussed previously. The difference between the true pressure distribution curve, and that obtained using equilibrium flow conditions will, therefore, be less than that shown in figure 15. Such a difference is not significant to the present data analysis, thus free-stream conditions for equilibrium flow will be used in the following figures.

Perfect-gas theories in blast-wave form.- The perfect-gas theories which describe cylinder pressure with equations in blast-wave form are compared with experiment in figure 16. The first- and second-order blast-wave approximations (eqs. (2) and (4), respectively) and the correlated perfect-gas characteristics solutions (eq. (8)) are shown with the present experiment, correlated on the basis of model stagnation γ. Agreement between theory, expressed in second-order blast-wave form, and experiment is good. It is interesting that theories so fundamentally different give predictions so similar.

Various investigations of the blast-wave theory have resulted in some differences of opinion with regard to the accuracy with which the theory will predict cylinder pressures. Generally, the theory has provided a fair prediction of pressures within the range of conditions for which it is intended to apply. Since blast-wave theory assumes an infinite blast pressure at the stagnation point and a strong bow shock, the theory should not be valid close to the nose or for long cylinders or low Mach numbers. Comparisons with experiment substantiate these limitations and show the theory to be good for $3 \lesssim x/D \lesssim 10$ and for $M_\infty \gtrsim 7$ if the correct γ is used (e.g., refs. 6, 15, and 24). The present experiments indicate that second-order blast theory (eq. (4)) also applies to real-air flow when the value of γ at the model stagnation point is used. Comparison of the second-order theory for $\gamma = 1.4$ with real-air characteristics solutions (refs. 6 and 25) does not show good agreement; however, good agreement would have resulted for values of $x/D > 2$ if the real-air stagnation γ had been used. The conclusion in reference 15 that blast-wave theory is inadequate except in very limited regions is not in conflict with the conclusions of references 6 and 24 and the present investigation because these conclusions apply to widely different ranges of x/D. The helium experiments (ref. 15) were for values of x/D to about 45; the other experiments were for x/D to 10. As stated previously, the blast-wave analogy assumptions do not apply far downstream; in addition viscous effects become significant there. Viscous effects will, of course, limit any inviscid theory, and are not a limitation peculiar to the blast-wave analogy. A serious limitation of the theory, the overprediction of pressure for x/D up to about 3, is reduced considerably if the blast origin is considered to occur ahead of the model (refs. 9 and 26); however, the proper amount to shift the origin can be determined only by examining many cases, since such a shift is not suggested by theory.

Perfect-gas characteristics solutions correlated by the blast-wave parameter (ref. 7 or eq. (6) of the present report) were compared with helium data in reference 16. The correlated characteristics solutions gave only a fair approximation to the helium data. It should be noted in examining the comparisons in reference 16, however, that proper comparison of the correlated characteristics solutions (eq. (6)) with experiment requires a shift to the left of the theoretical curve an amount equivalent to the nose length. This is necessary because the difference in coordinate origin in references 7 and 16 was not accounted for in reference 16. Such a shift improves the agreement between theory and experiment near the nose; the disagreement downstream can be attributed to viscous effects. The result of these comparisons is, therefore, consistent with the results of other such comparisons mentioned previously.

Pressure-decay method.- The pressure-decay equation (eq. (9)) generally provides a fair estimate of the cylinder pressure if the value used for shoulder pressure is properly chosen (e.g., refs. 6, 12, 15, 16, 25, and 26, and figs. 17

and 18). Figure 17 illustrates that the present experimental pressure distributions are qualitatively described by equation (9) when the values of shoulder pressure are determined as discussed in the section, Theories for Determining Cylinder Pressures. Obviously, these values of shoulder pressure were too low to give a favorable quantitative comparison with experiment. Since the initial pressure, p_s/p_∞, is subject to arbitrary selection, a curve is shown in figure 17 for a value of initial pressure which was chosen to give good agreement with experiment. This comparison does not demonstrate the present capabilities of equation (9), but it does show the quality of agreement possible if the proper initial pressure is used. In addition this comparison shows that the pressure decay given by equation (9) is indeed very similar to the blast analogy (cf. figs. 16 and 17). Figure 18 is typical of many comparisons made in the present investigation of this method with characteristics solutions by Edsall, Vaglio-Laurin and Trella, and Inouye and Lomax. Often a better estimation of cylinder pressure results if the pressure used in equation (9) is greater than the shoulder pressure. Perhaps shoulder pressure is not the best reference value for the equation; instead, it might be more appropriate to refer to another initial pressure from which the decay process begins. The flexibility of the equation attained through the arbitrary initial pressure is an advantage which could result in a good estimation of cylinder pressure for a wide range of conditions, but on the other hand, this same flexibility presents a problem in the use of equation (9). The weak point of equation (9) is, of course, the lack of information on the proper initial pressure for various geometries, Mach numbers, and values of the isentropic exponent. Presently, a fair estimate can be made of cylinder pressure for hemisphere-cylinders, but extension of the method to other blunt cylinders will require additional knowledge of the proper initial pressure.

Real-air theories.- The characteristics method and the flow-continuity method have been used to compute cylinder pressures for the case of equilibrium flow of real air. These solutions are shown in figure 19. Other comparisons of these theories with real-air experiment are not available. The one real-air characteristics solution available for the present test conditions is for a hemisphere-cylinder with a sonic starting cone. This theoretical solution agrees well with the experiment for blunt cylinders (fig. 19). The prediction of experimental pressures by the continuity method is not satisfactory because of the large error in the rate of pressure decay. This is somewhat surprising since reference 11 shows a favorable comparison of the flow properties between body and shock for the continuity and characteristics methods. Although not presented here, other comparisons of theoretical surface pressures show that the continuity prediction crosses over that of characteristics solutions in the same manner as exhibited in figure 19; thus this crossover is not peculiar to the experimental data. Further, close examination of the theoretical comparisons in reference 11 also indicates this crossover. The favorable comparisons of flow-field properties in reference 11 and the adverse comparisons of surface pressure in figure 19 are, however, not inconsistent because the former comparisons were made in the region where the prediction of surface pressure was good, that is, near the crossover point of the pressure distributions. It is possible that flow-field properties might not compare as well farther away from this crossover point. In fact, a likely reason why this method was consistently low near the nose and high downstream could be that the distribution of the static pressure between body and shock was not constant, as assumed in the theory, but instead varied along the

cylinder. In addition to the tendency of the pressure distributions to cross over, the three continuity calculations do not correlate among themselves. A possible factor contributing to the lack of correlation could be that the experimental shock wave used in the continuity calculation was obtained in a conical stream rather than the assumed uniform stream. The calculated pressure jump across the shock would, therefore, be in slight error. It seems, however, that this error must necessarily be of different magnitude for each of the three models to cause the observed lack of correlation of the continuity calculations. Nevertheless, the continuity method did not predict surface pressure as accurately as other methods which were easier to use.

CONCLUSIONS

1. The blast-wave parameter provided a good correlation of cylinder pressures for a wide range of isentropic exponent, Mach number, and nose drag in perfect gases and real air.

2. The second-order blast analogy and the perfect-gas characteristics solutions correlated in blast-wave form gave good predictions of the real air, experimental cylinder pressures.

3. The real-air characteristics solution of a blunt body with a sonic starting cone gave a good prediction of the experimental pressures.

Ames Research Center
National Aeronautics and Space Administration
Moffett Field, Calif., June 19, 1963

REFERENCES

1. Gowen, Forrest E., and Hopkins, Vaughn D.: A Wind Tunnel Using Arc-Heated Air for Mach Numbers From 10 to 20. Advances in Hypervelocity Techniques, Arthur M. Krill, ed. Proc. Second Symposium on Hypervelocity Techniques, Denver, March 20-21, 1962, Plenum Press, N. Y., pp. 27-46.

2. Jorgensen, Leland H., and Baum, Gayle M.: Charts for Equilibrium Flow Properties of Air in Hypervelocity Nozzles. NASA TN D-1333, 1962.

3. Shepard, Charles E., and Winovich, Warren: Electric-Arc Jets for Producing Gas Streams With Negligible Contamination. ASME Paper 61-WA-247.

4. Moeckel, W. E., and Weston, Kenneth C.: Composition and Thermodynamic Properties of Air in Chemical Equilibrium. NACA TN 4265, 1958.

5. Landis, F., and Nilson, E. N.: Thermodynamic Properties of Ionized and Dissociated Air From 1500° K to 15,000° K. Rep. 1921, Pratt and Whitney, Aircraft, Jan. 1961.

6. Lukasiewicz, J.: Hypersonic Flow-Blast Analogy, AEDC TR 61-4, 1961.

7. Van Hise, Vernon: Analytic Study of Induced Pressure on Long Bodies of Revolution With Varying Nose Bluntness at Hypersonic Speeds. NASA TR R-78, 1961.

8. Edsall, R. H.: Calculation of Flow Fields About Blunt Bodies of Revolution Traveling at Escape Velocity. ARS Paper 2492-62.

9. Vaglio-Laurin, Roberto, and Trella, Massimo: A Study of Flow Fields About Some Typical Blunt-Nosed Slender Bodies. PIBAL Rep. 623, Polytechnic Institite of Brooklyn, 1960.

10. Inouye, Mamoru, and Lomax, Harvard: Comparison of Experimental and Numerical Results for the Flow of a Perfect Gas About Blunt-Nosed Bodies. NASA TN D-1426, 1962.

11. Seiff, Alvin, and Whiting, Ellis E.: Calculation of Flow Fields From Bow-Wave Profiles for the Downstream Region of Blunt-Nosed Circular Cylinders in Axial Hypersonic Flight. NASA TN D-1147, 1961.

12. Love, E. S.: Prediction of Inviscid Induced Pressures From Round Leading Edge Blunting at Hypersonic Speeds. American Rocket Society Jour., vol. 29, no. 10, Oct. 1959, pp. 792-794.

13. Sakurai, Akira: On the Propagation and Structure of the Blast Wave, I. Jour. Phys. Soc. of Japan, vol. 8 no. 5, Sept. - Oct. 1953, pp. 662-669.

14. Kuehn, Donald M.: Blast-Wave Correlation of Pressures on Blunt-Nosed Cylinders in Perfect- and Real-Gas Flows at Hypersonic Speeds. American Institute of Aeronautics and Astronautics Jour., vol. 1, no. 3, Mar. 1963, pp. 716-717.

15. Mueller, James N., Close, William H., and Henderson, Arthur, Jr.: An Investigation of Induced-Pressure Phenomena on Axially Symmetric, Flow-Alined, Cylindrical Models Equipped With Different Nose Shapes at Free-Stream Mach Numbers From 15.6 to 21 in Helium. NASA TN D-373, 1960.

16. Witcofski, Robert D., and Henderson, Arthur, Jr.: Induced Pressures on Cylindrical Rods With Various Nose Drags and Nose Shapes at Mach Numbers of 17 and 21. NASA TN D-1266, 1962.

17. Probstein, Ronald F., and Kemp, Nelson H.: Viscous Aerodynamic Characteristics in Hypersonic Rarefied Gas Flow. Jour. Aero/Space Sci., vol. 27, no. 3, March 1960, pp. 174-192, 218.

18. Ho, Hung-Ta, and Probstein, Ronald F.: The Compressible Viscous Layer in Rarefied Hypersonic Flow. Brown Univ., Div. of Engineering. ARL-TN-60-132, August 1960.

19. Jeans, Sir James: The Dynamical Theory of Gases. 4th ed., Dover Pub., Inc., New York, 1954.

20. Hermann, Rudolf: Problems of Hypersonic Flight at the Re-Entry of Satellite Vehicles. Research Rep. 153, Rosemount Aeronautical Labs., University of Minnesota, Nov. 1958.

21. Blackman, Vernon: Vibrational Relaxation in Oxygen and Nitrogen. Jour. Fluid Mech., vol. 1, pt. 1, May 1956, pp. 61-85.

22. Kaattari, George E.: Predicted Shock Envelopes About Two Types of Vehicles at Large Angles of Attack. NASA TN D-860, 1961.

23. Van Dyke, Milton D., and Gordon, Helen D.: Supersonic Flow Past a Family of Blunt Axisymmetric Bodies. NASA TR R-1, 1959.

24. Kubota, Toshi: Investigation of Flow Around Simple Bodies in Hypersonic Flow. GALCIT Memo. 40, 1957.

25. Love, Eugene S.: Comparisons of Modified Blast Wave Estimate of Induced Pressures With Real Gas Solutions. American Rocket Society Journal, vol. 32, no. 6, June 1962, pp. 956-957.

26. Lukasiewicz, J.: Blast-Hypersonic Flow Analogy Theory and Application. American Rocket Society Journal, vol. 32, no. 9, Sept. 1962, pp. 1341-1346.

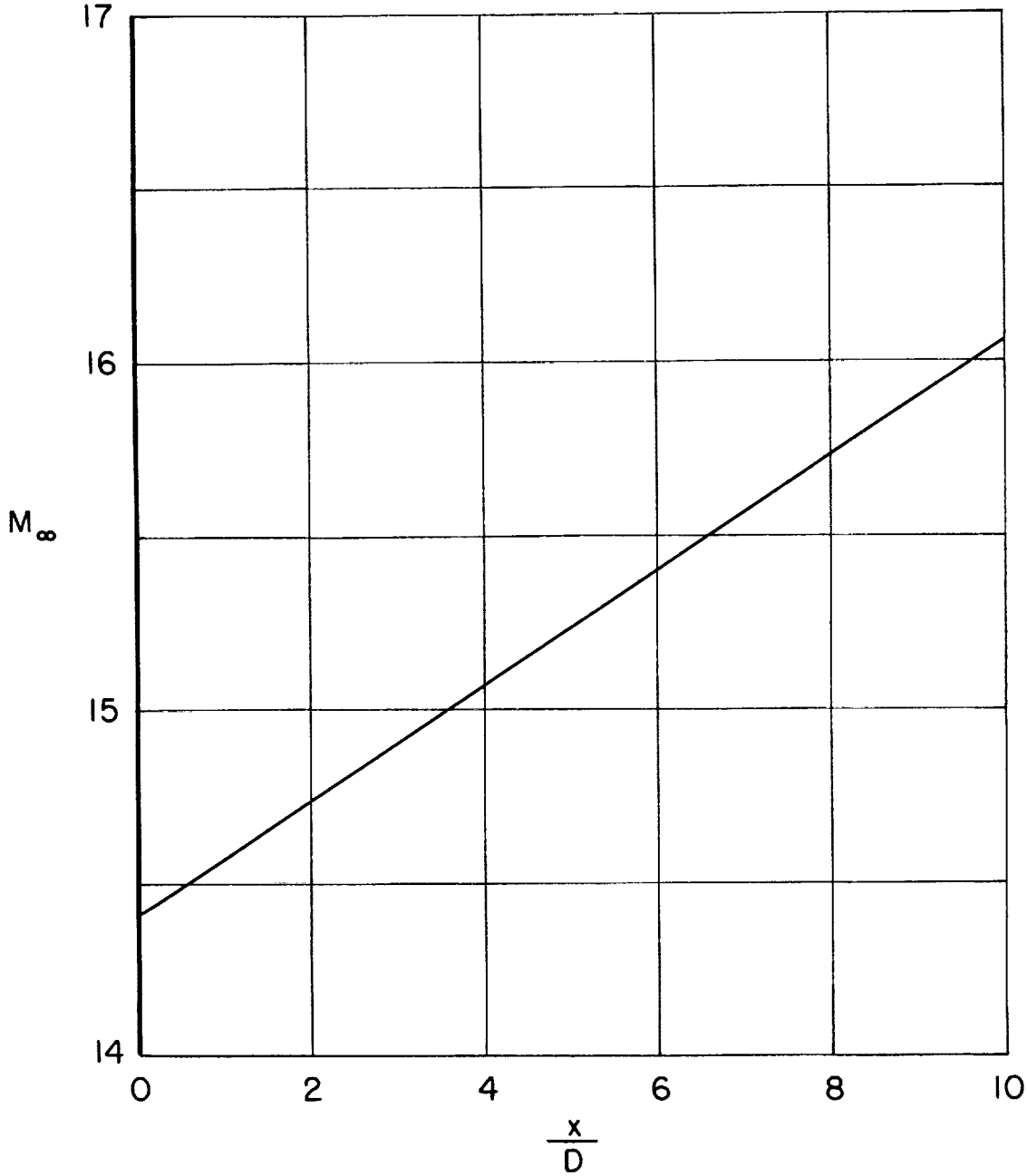

Figure 1.- Mach number distribution along the nozzle center line.

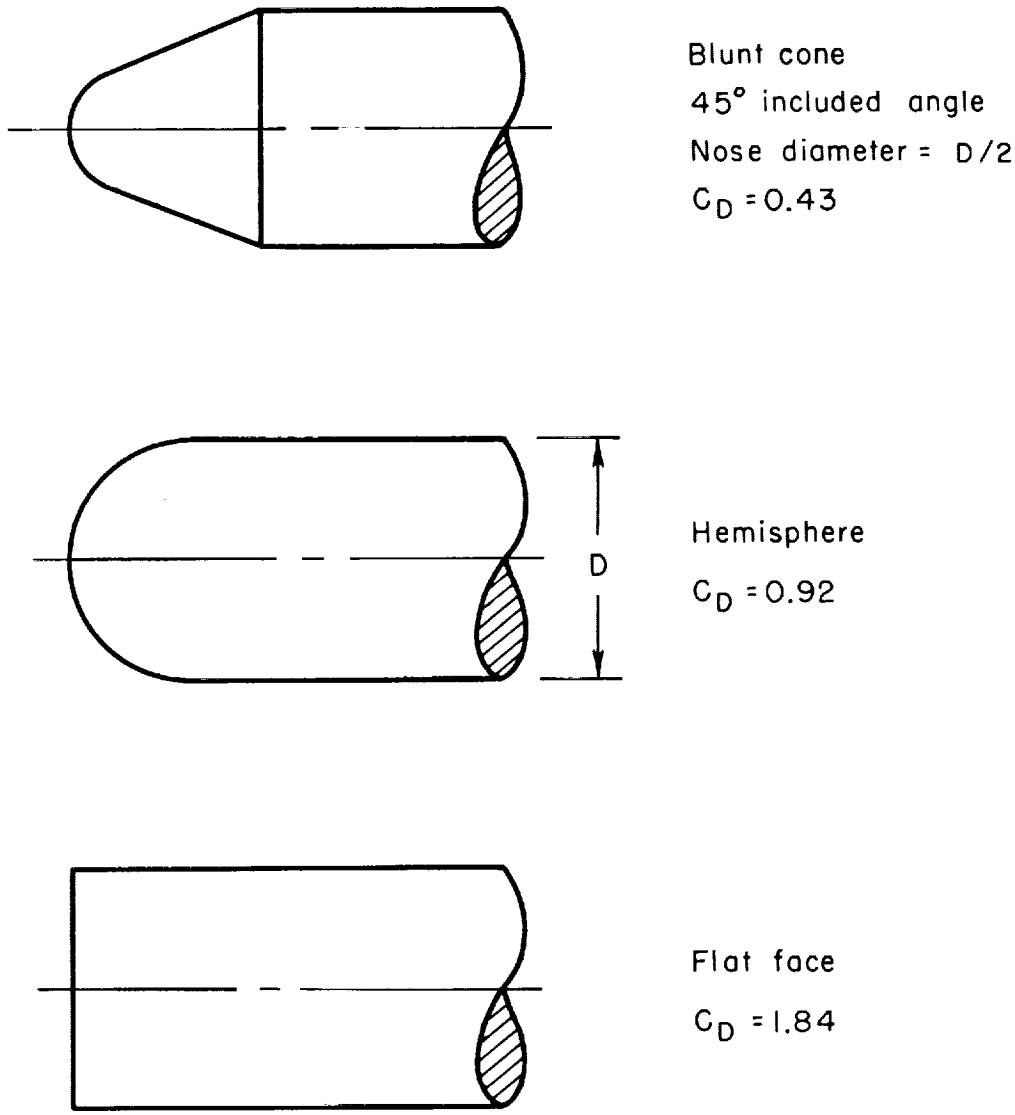

D = 0.625 inch
C_D -- Modified Newtonian drag coefficient

Figure 2.- Nose shapes for the stream-alined cylinder.

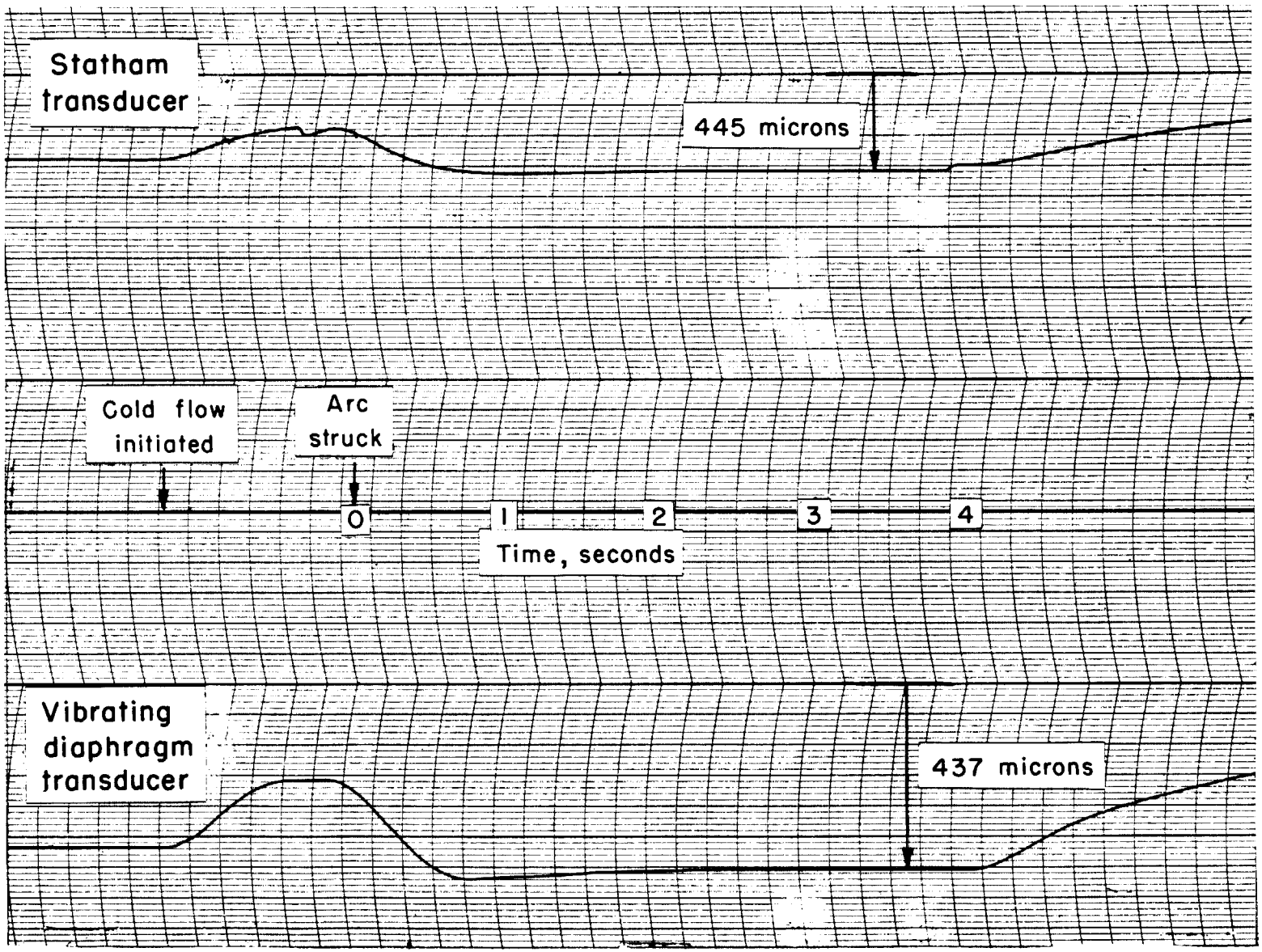

Figure 3.- Typical pressure traces.

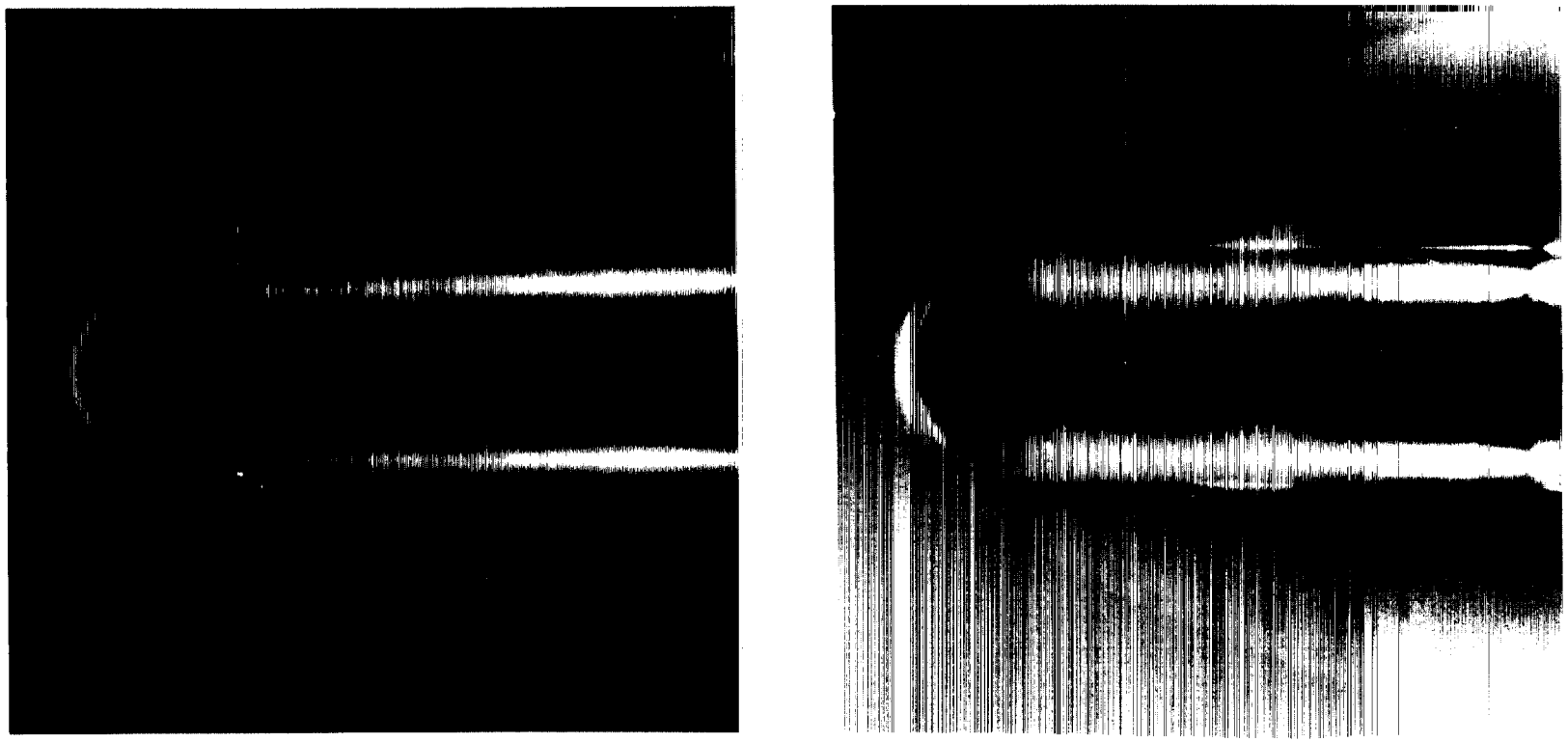

(a) Blunt cone-cylinder.

(b) Hemisphere-cylinder.

Figure 4.- Glow-discharge photographs.

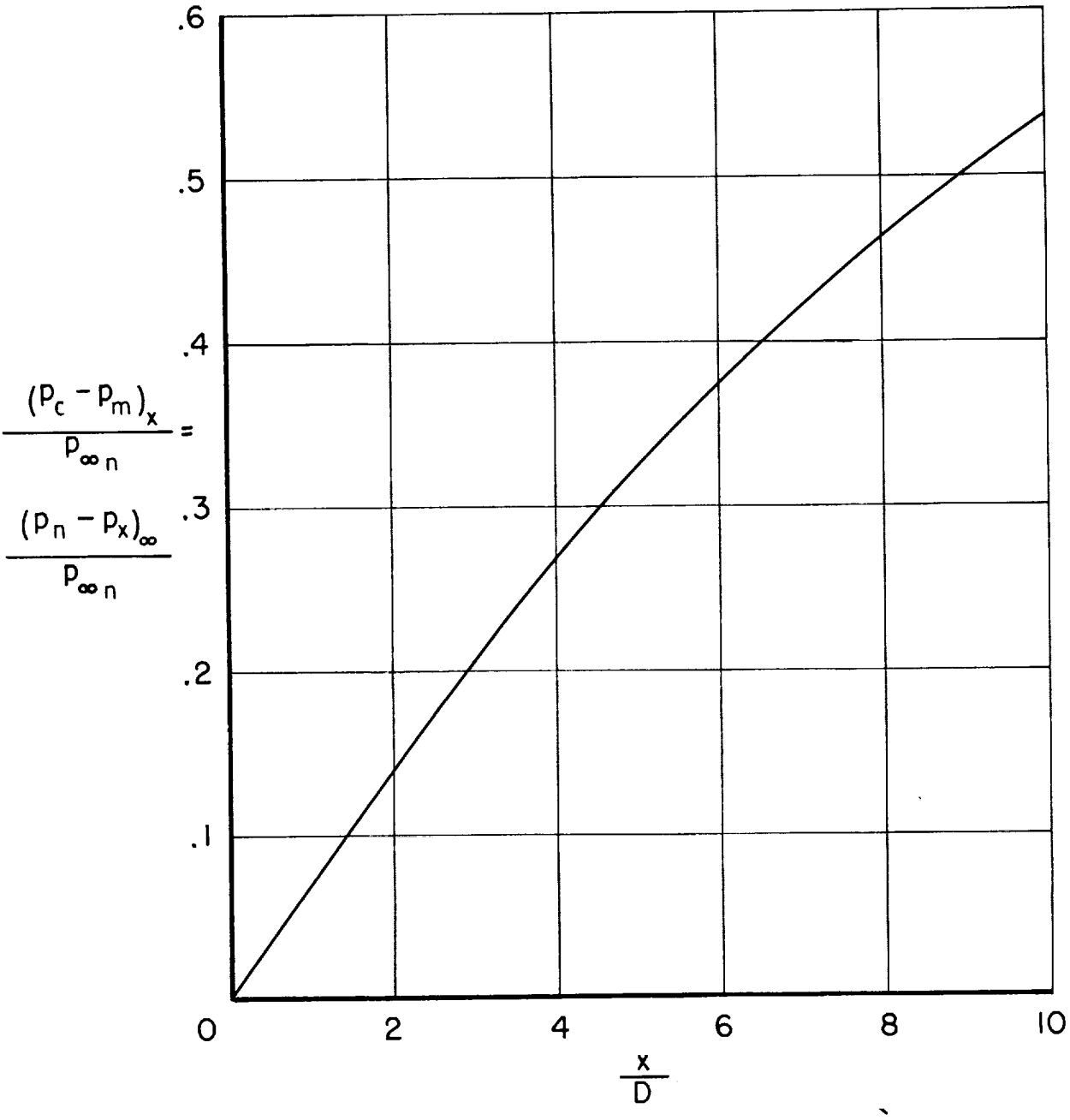

Figure 5.- Correction to measured static pressure due to center-line stream gradient.

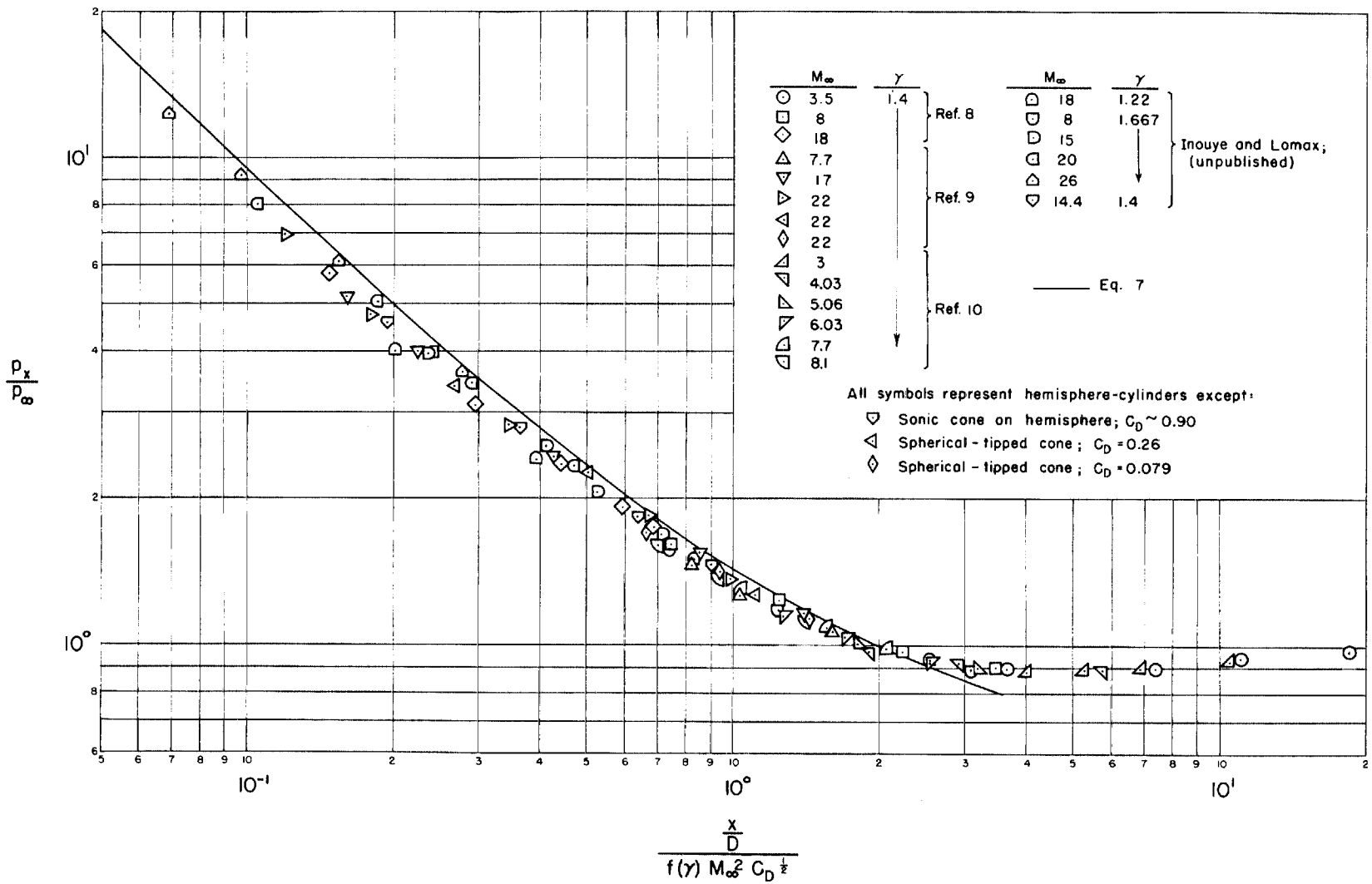

Figure 6.- Blast-wave correlation of perfect-gas characteristics solutions.

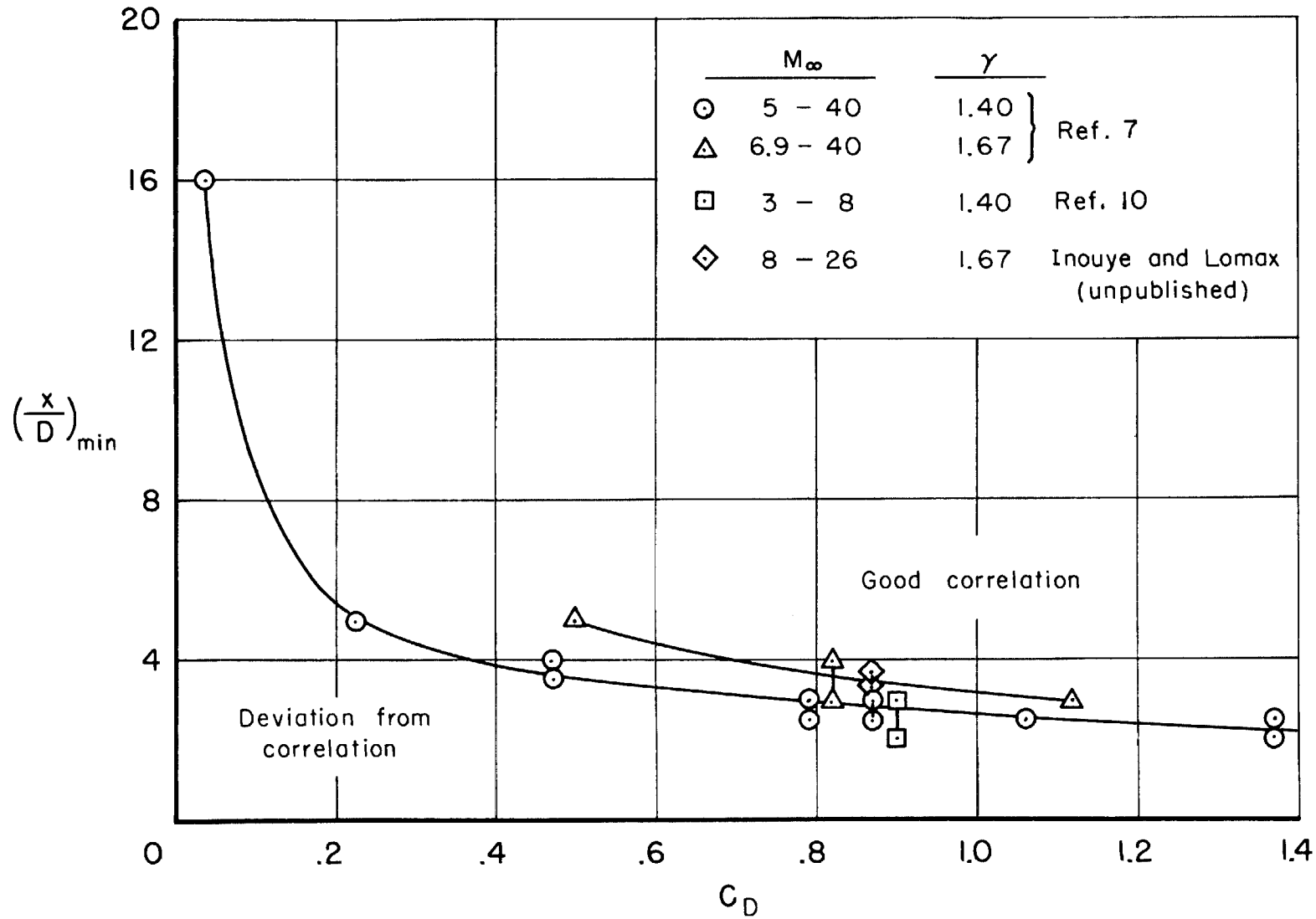

(a) Limits for two values of γ.

Figure 7.- A limitation to the validity of the blast-wave correlation of perfect-gas characteristics solutions.

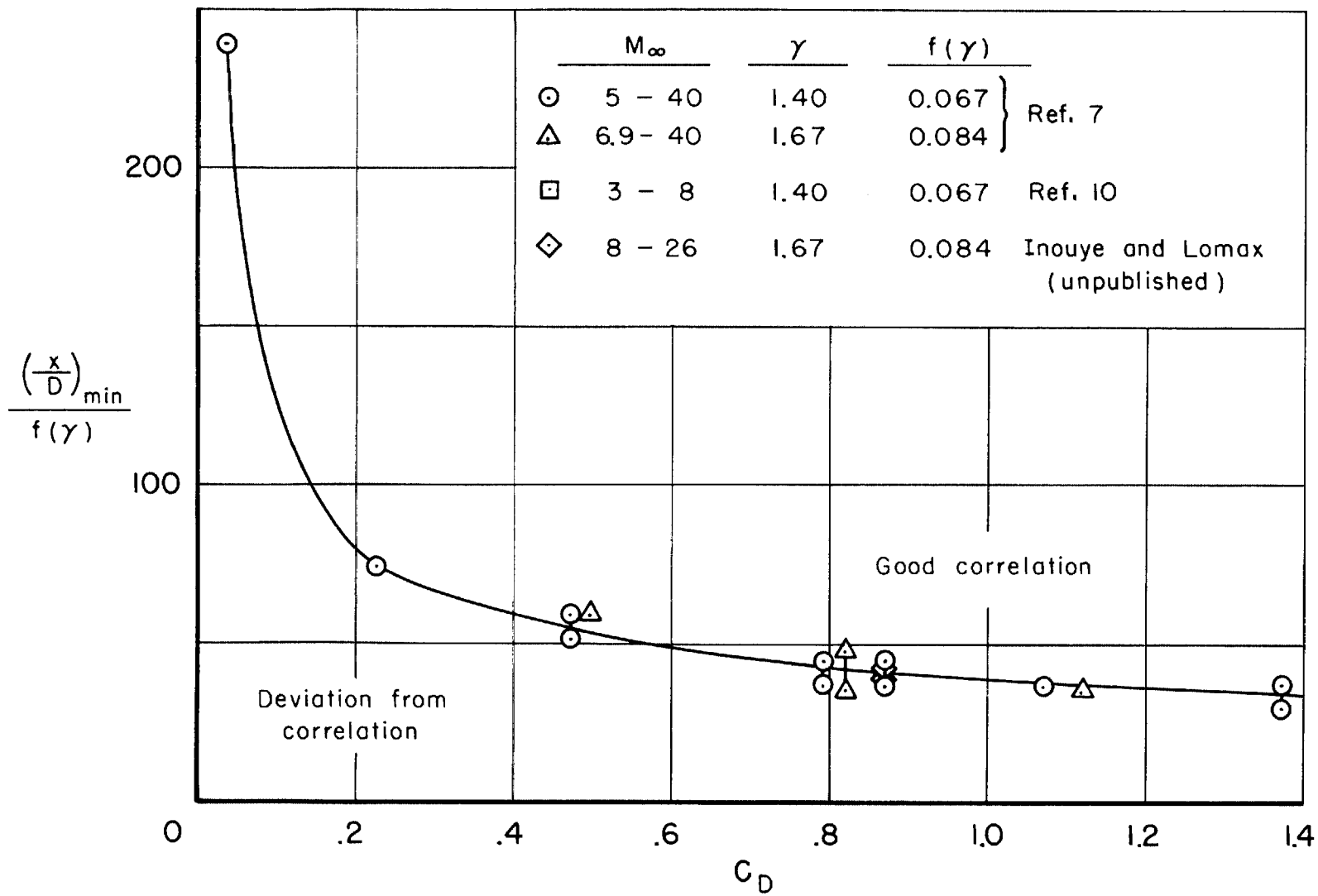

(b) Limits correlated for two values of γ.

Figure 7.- Concluded.

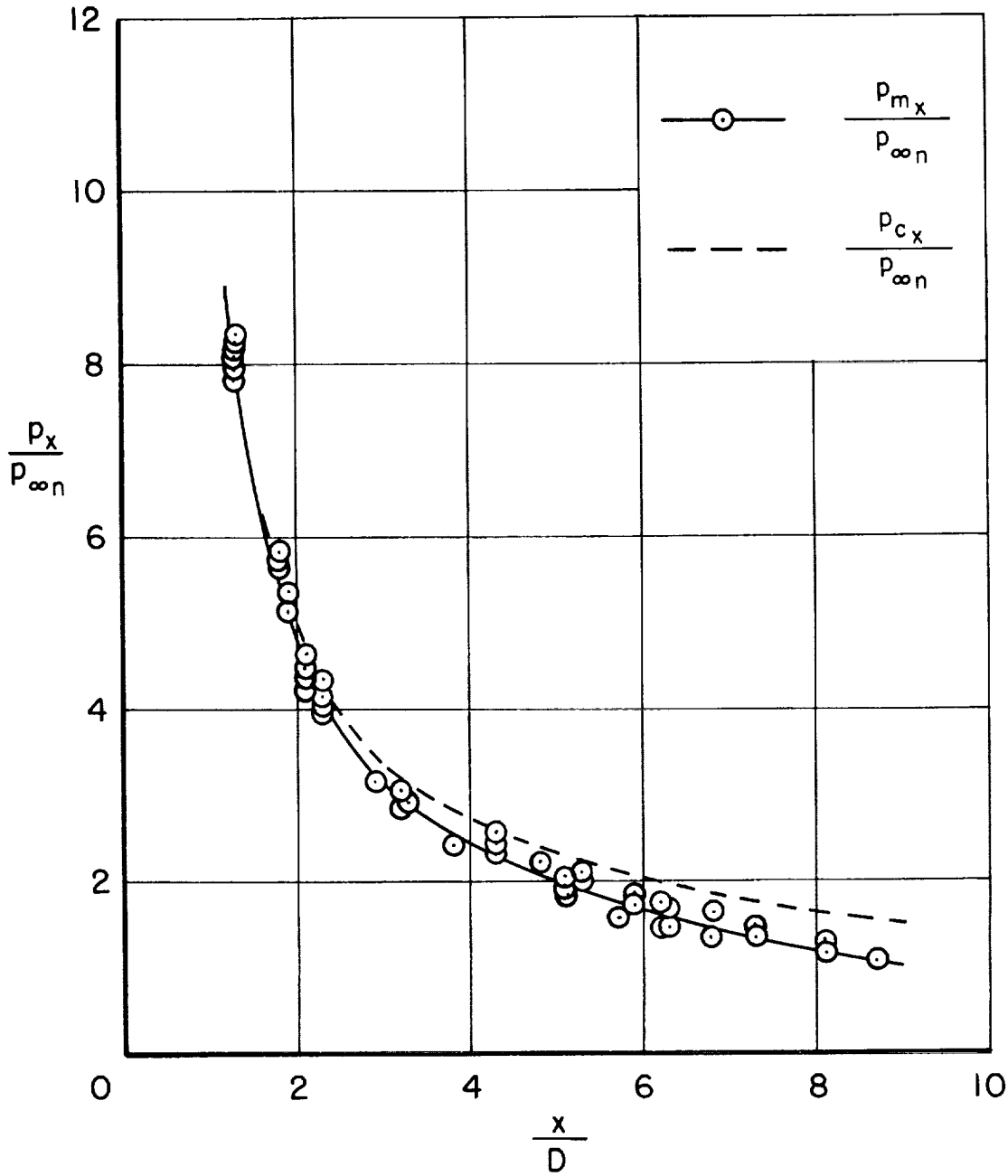

(a) Blunt cone-cylinder; p_{t_1} = 1000 psia, R_{∞_D} = 6200.

Figure 8.- Experimental pressure distributions induced by blunt noses on stream-alined cylinders; M_{∞_n} = 14.4, h_t = 1000 Btu/lb.

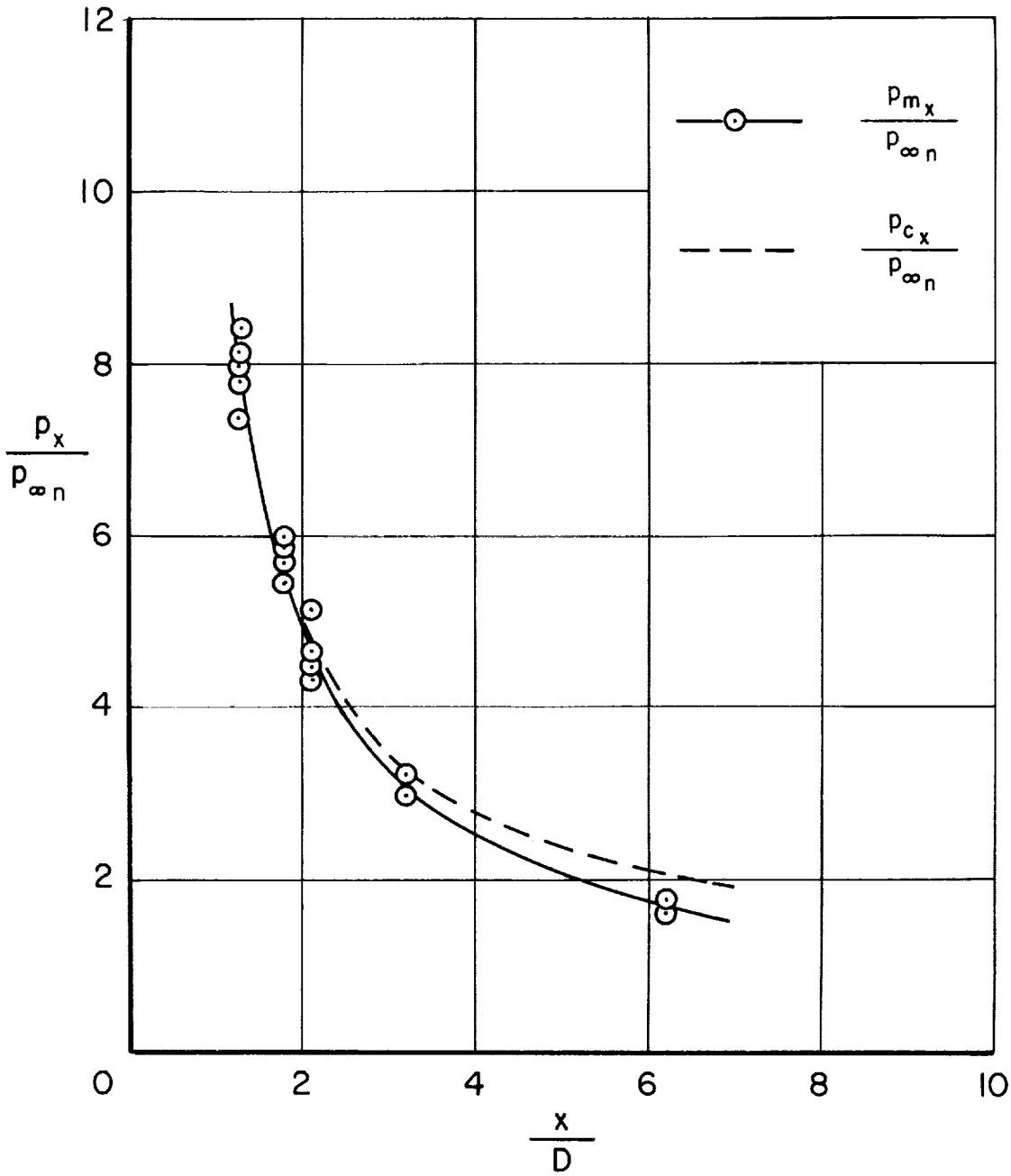

(b) Blunt cone-cylinder; p_{t_1} = 380 psia, R_{∞_D} = 2400.

Figure 8.- Continued.

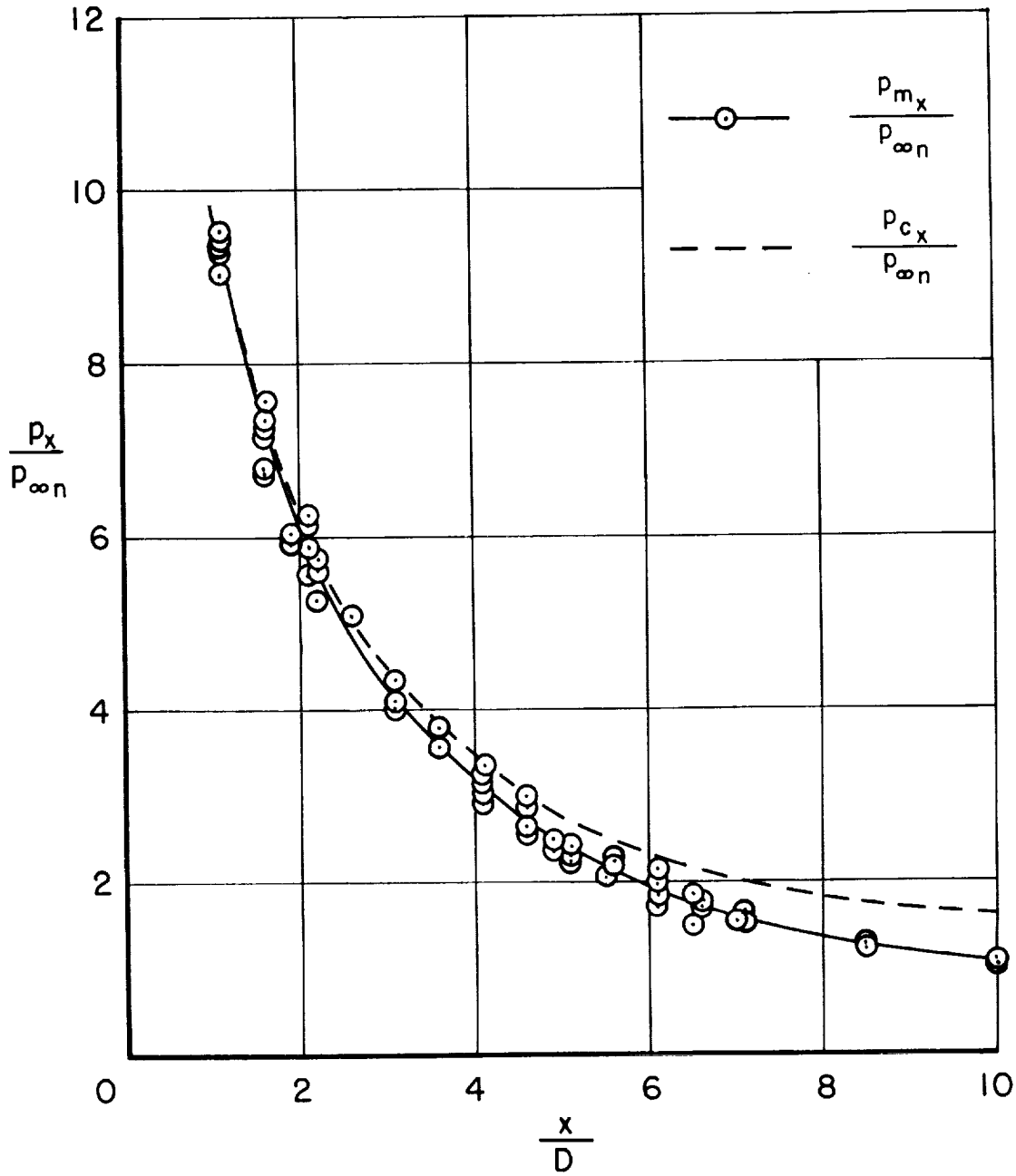

(c) Hemisphere-cylinder; p_{t_1} = 1000 psia, R_{∞_D} = 6200.

Figure 8.- Continued.

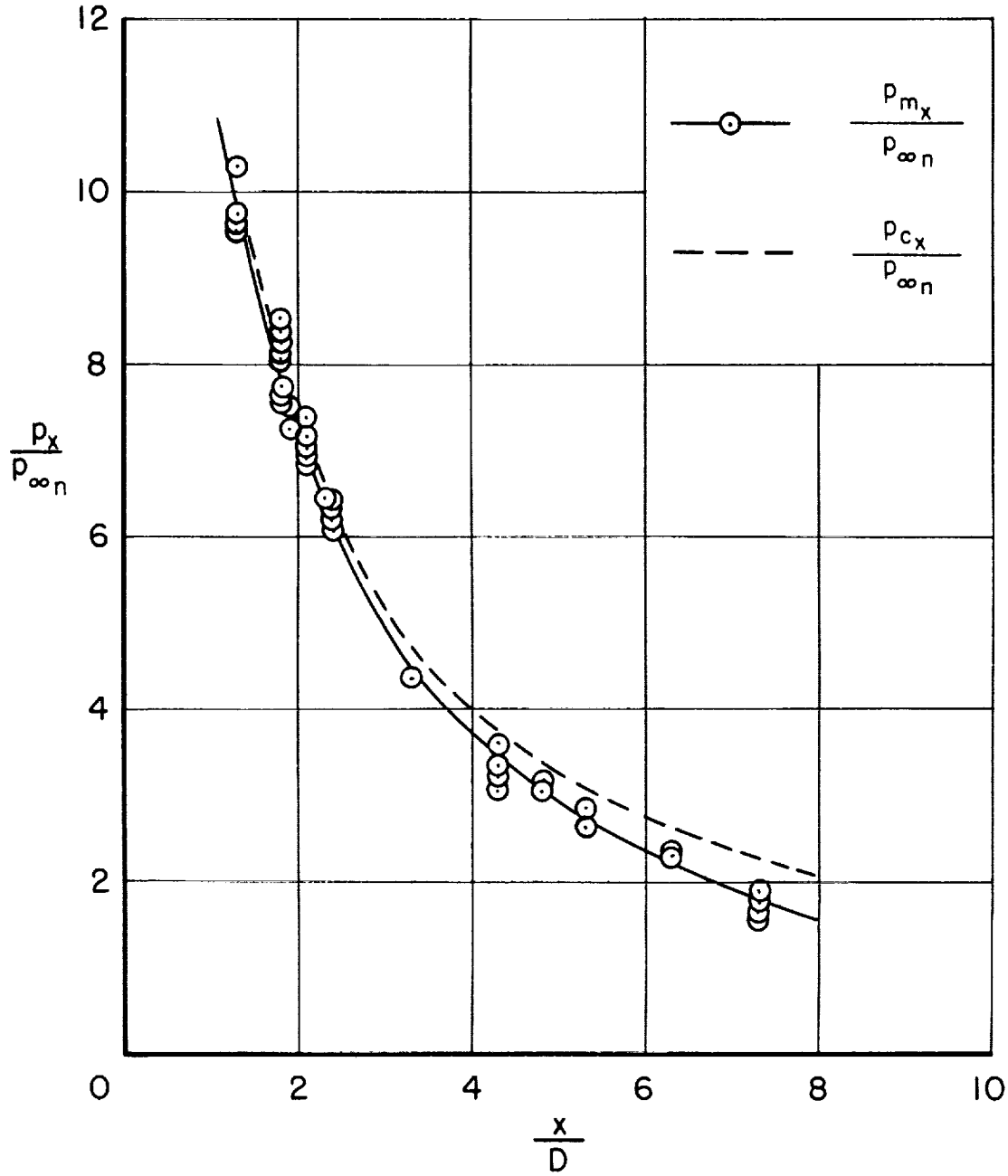

(d) Flat-face cylinder; p_{t_1} = 1000 psia, R_{∞_D} = 6200.

Figure 8.- Concluded.

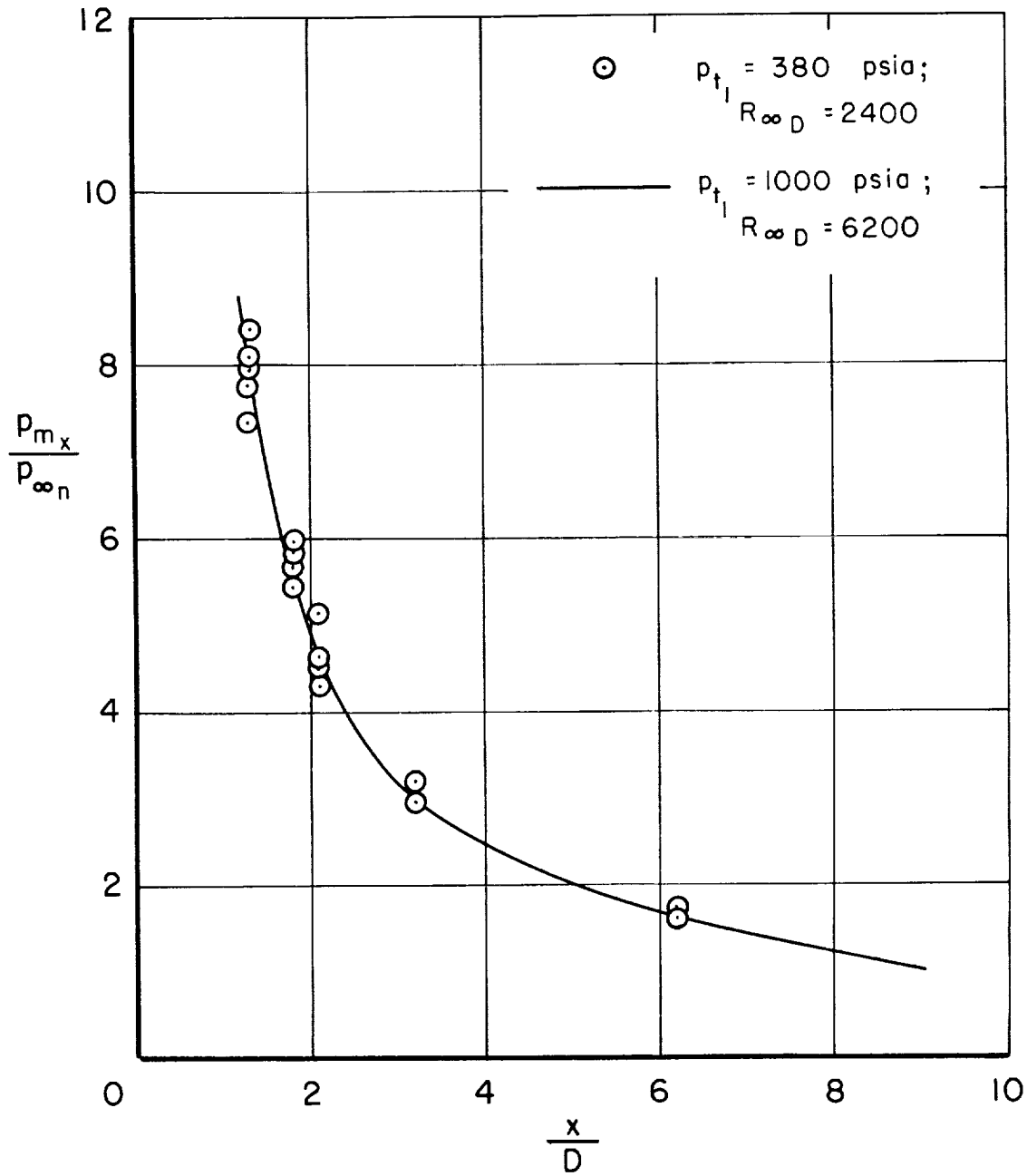

Figure 9.- Comparison of pressure distributions on the blunt cone-cylinder for two values of Reynolds number.

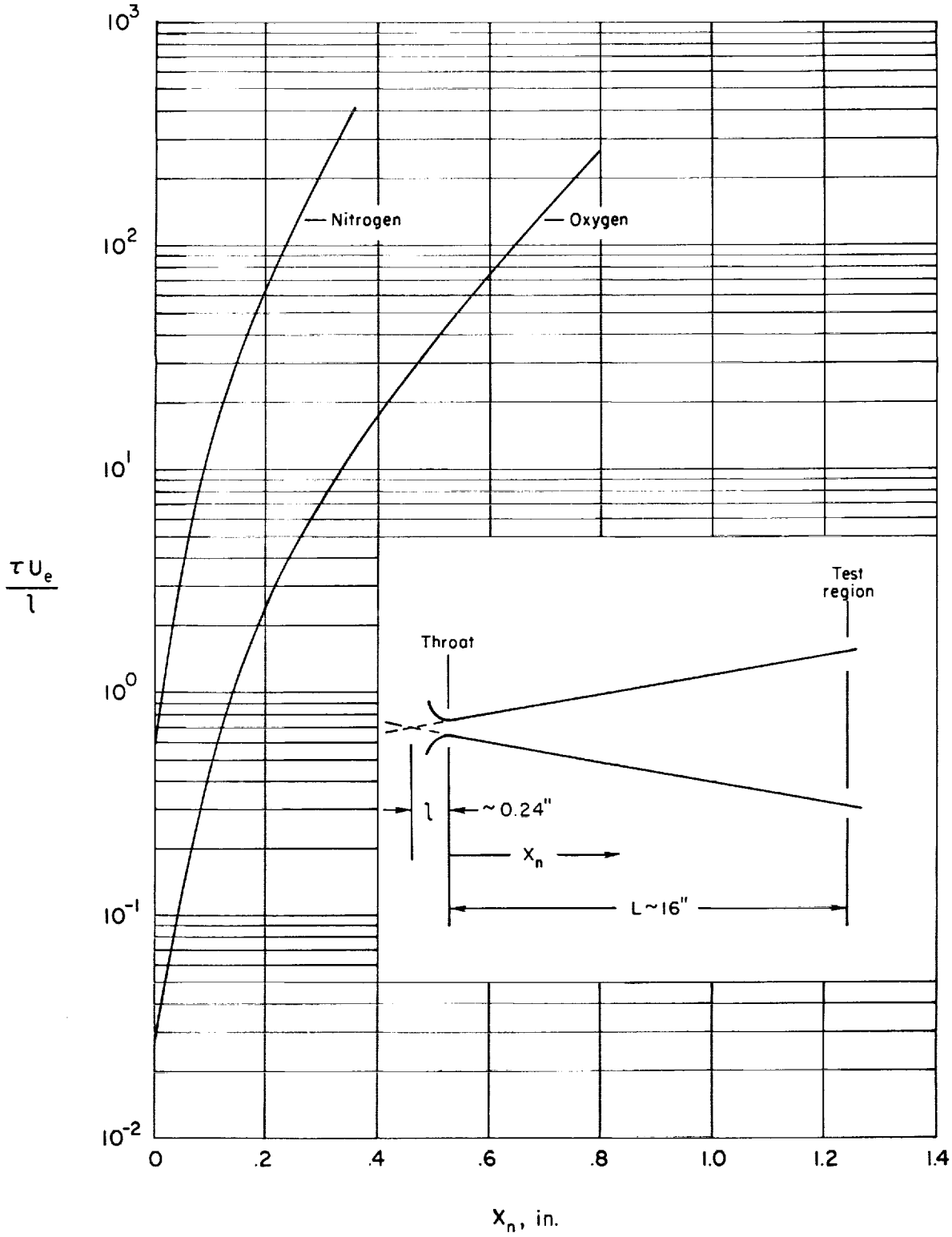

Figure 10.- Relaxation distance in the conical test nozzle using relaxation times for nitrogen and oxygen.

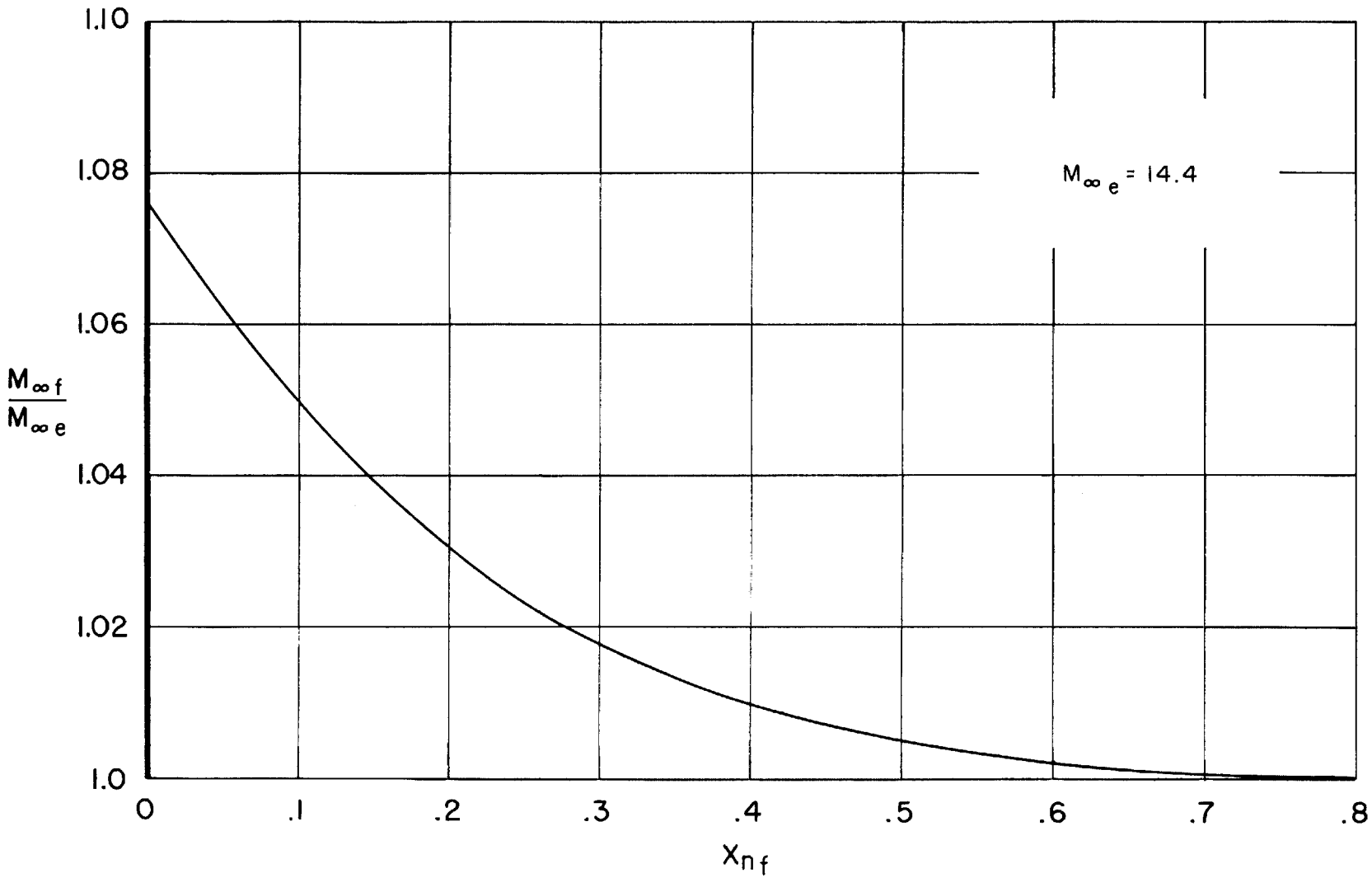

Figure 11.- Theoretical free-stream Mach number in the test region for various locations of vibrational freeze in the nozzle.

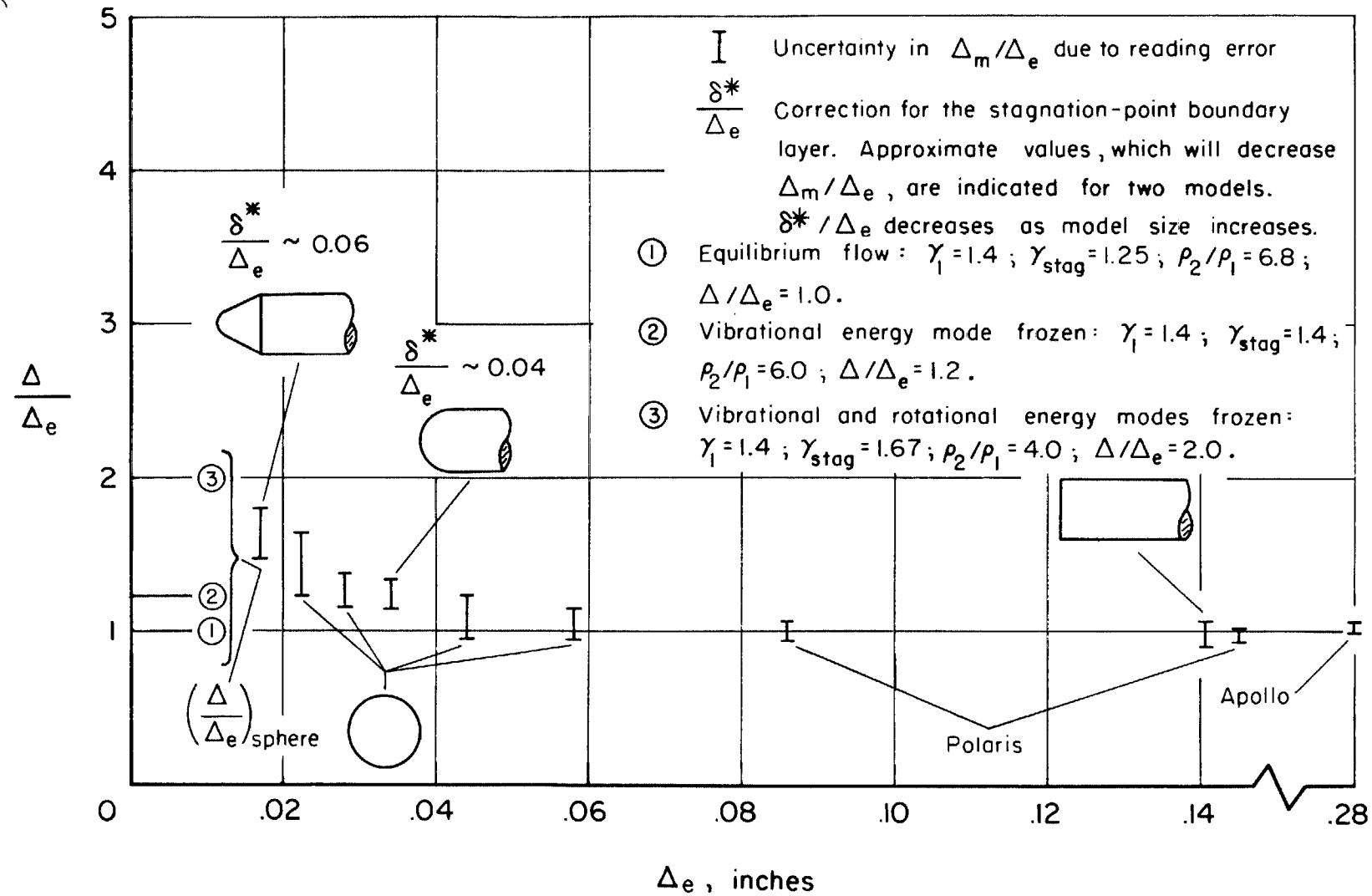

Figure 12.- Shock-standoff distances.

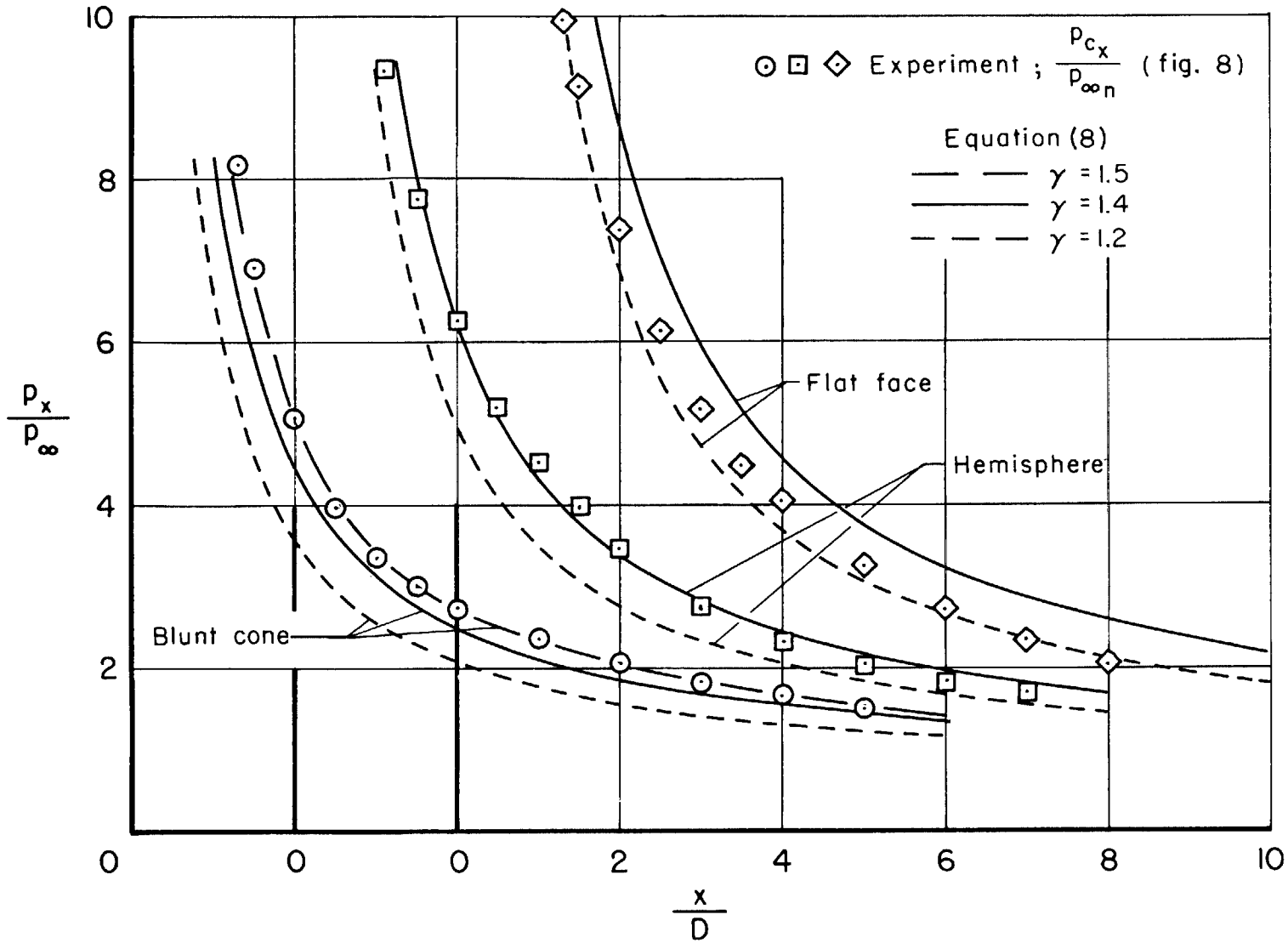

Figure 13.- Comparison of experiment and theory which indicates a variation of isentropic exponent for the experimental data; $M_{\infty_n} = 14.4$.

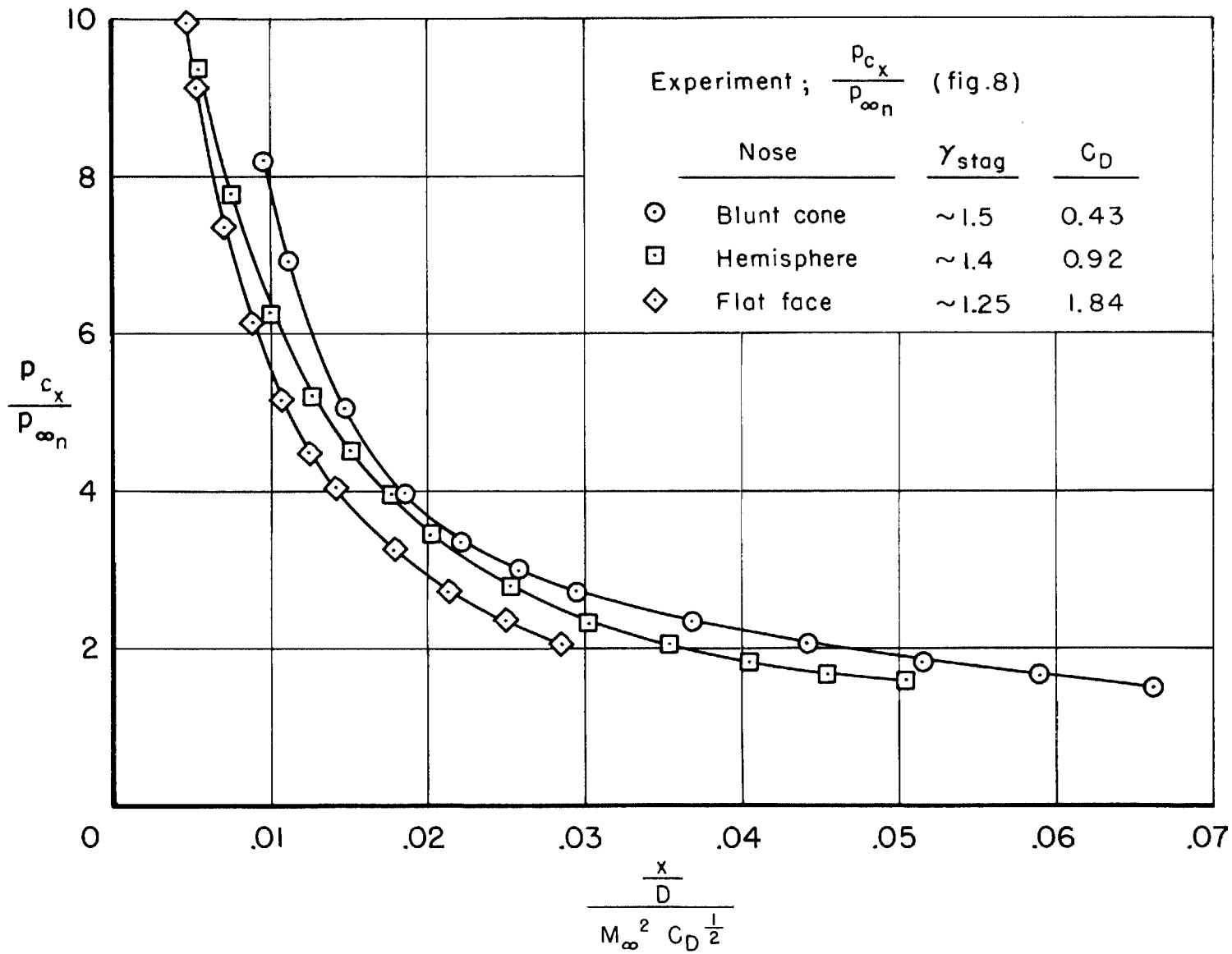

(a) Blast-wave parameter without the γ function.

Figure 14.- Blast-wave correlation of experimental pressures for real air; $M_{\infty_n} = 14.4$.

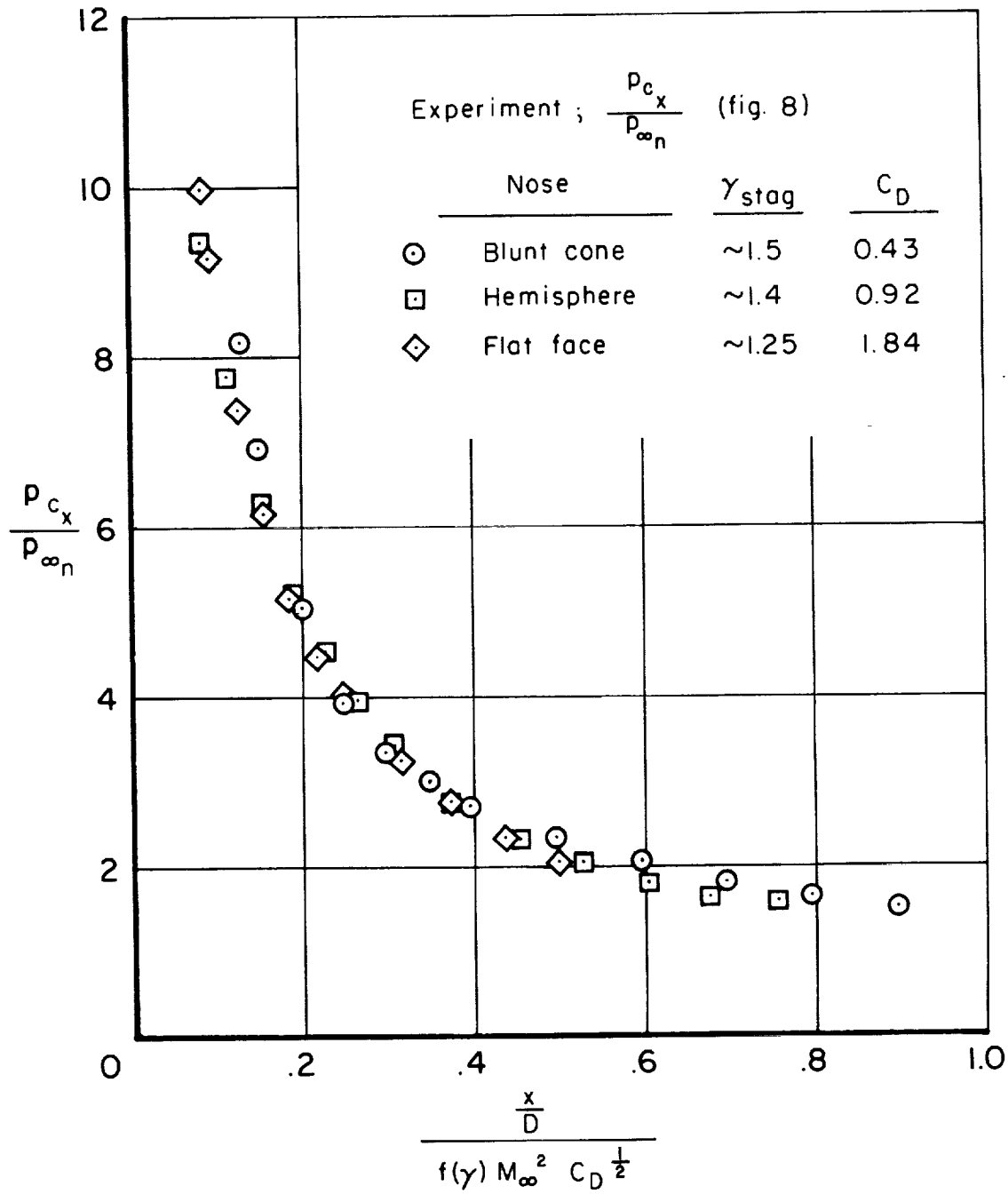

(b) Blast-wave parameter with γ function.

Figure 14.- Concluded.

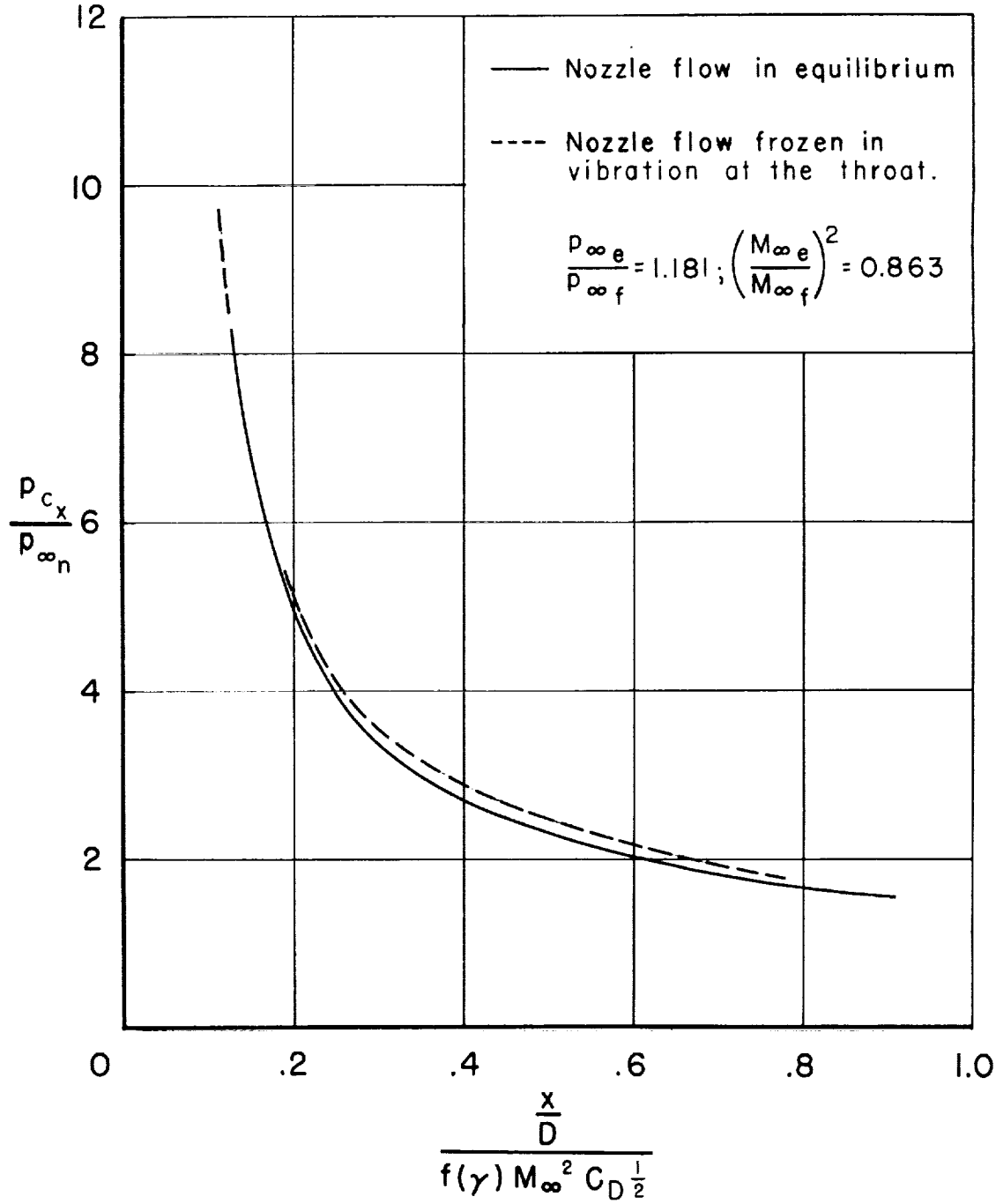

Figure 15.- Pressure distribution on the blunt cone-cylinder model referred to free-stream properties for nozzle flow in equilibrium and frozen.

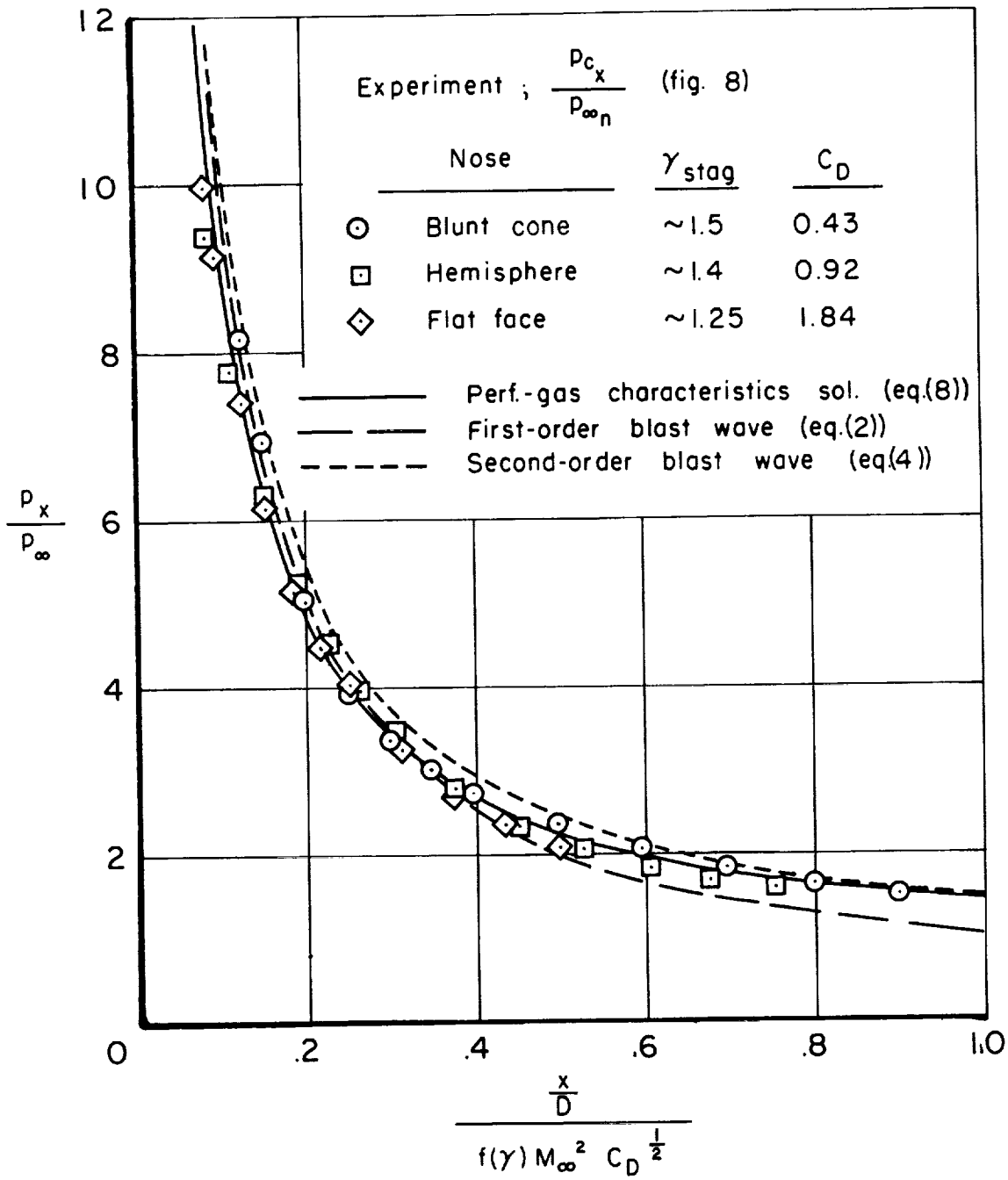

Figure 16.- Experiment compared with blast-wave theory and perfect-gas characteristics solutions; $M_{\infty_n} = 14.4$.

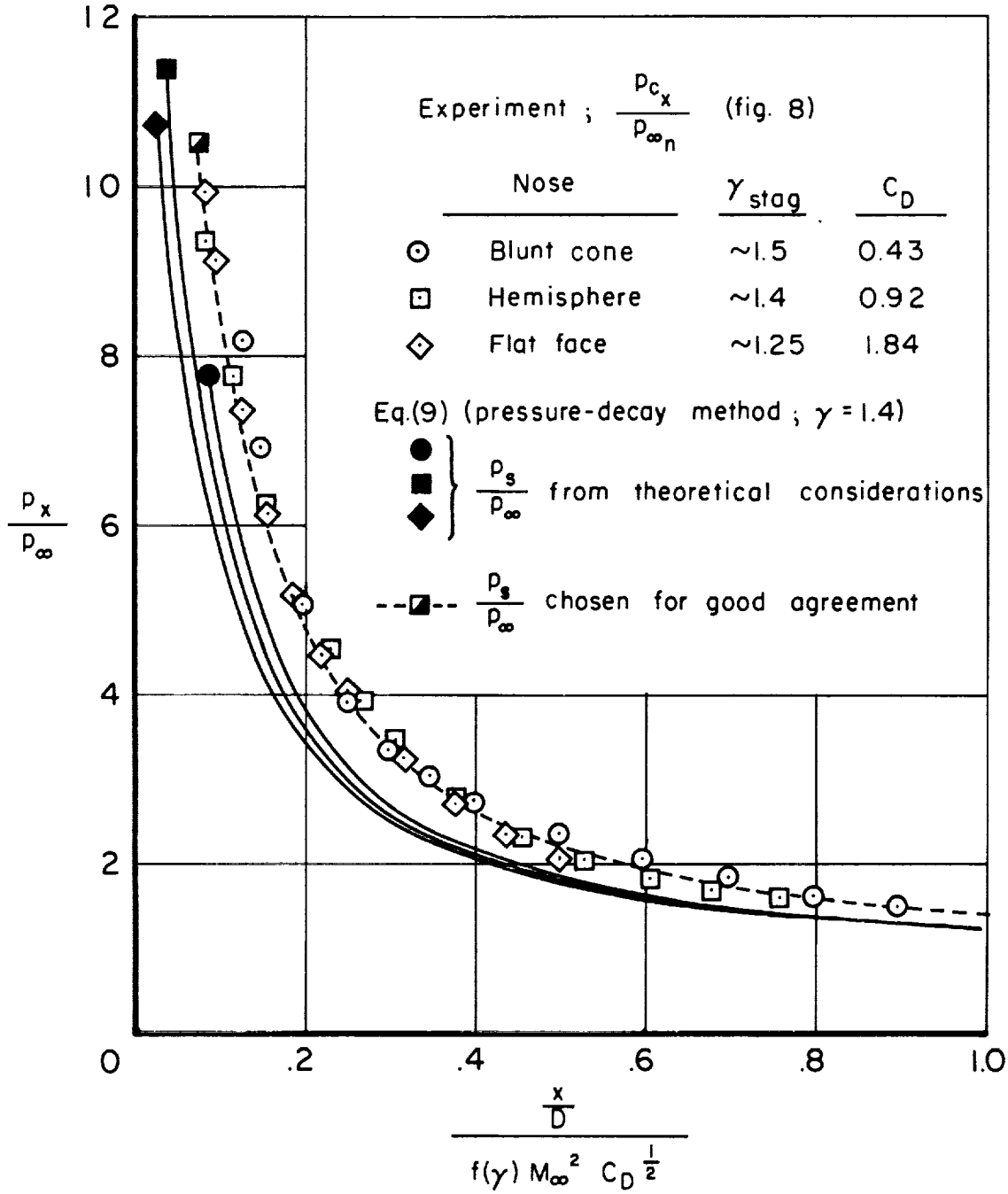

Figure 17.- Experiment compared with the pressure-decay method; $M_{\infty_n} = 14.4$.

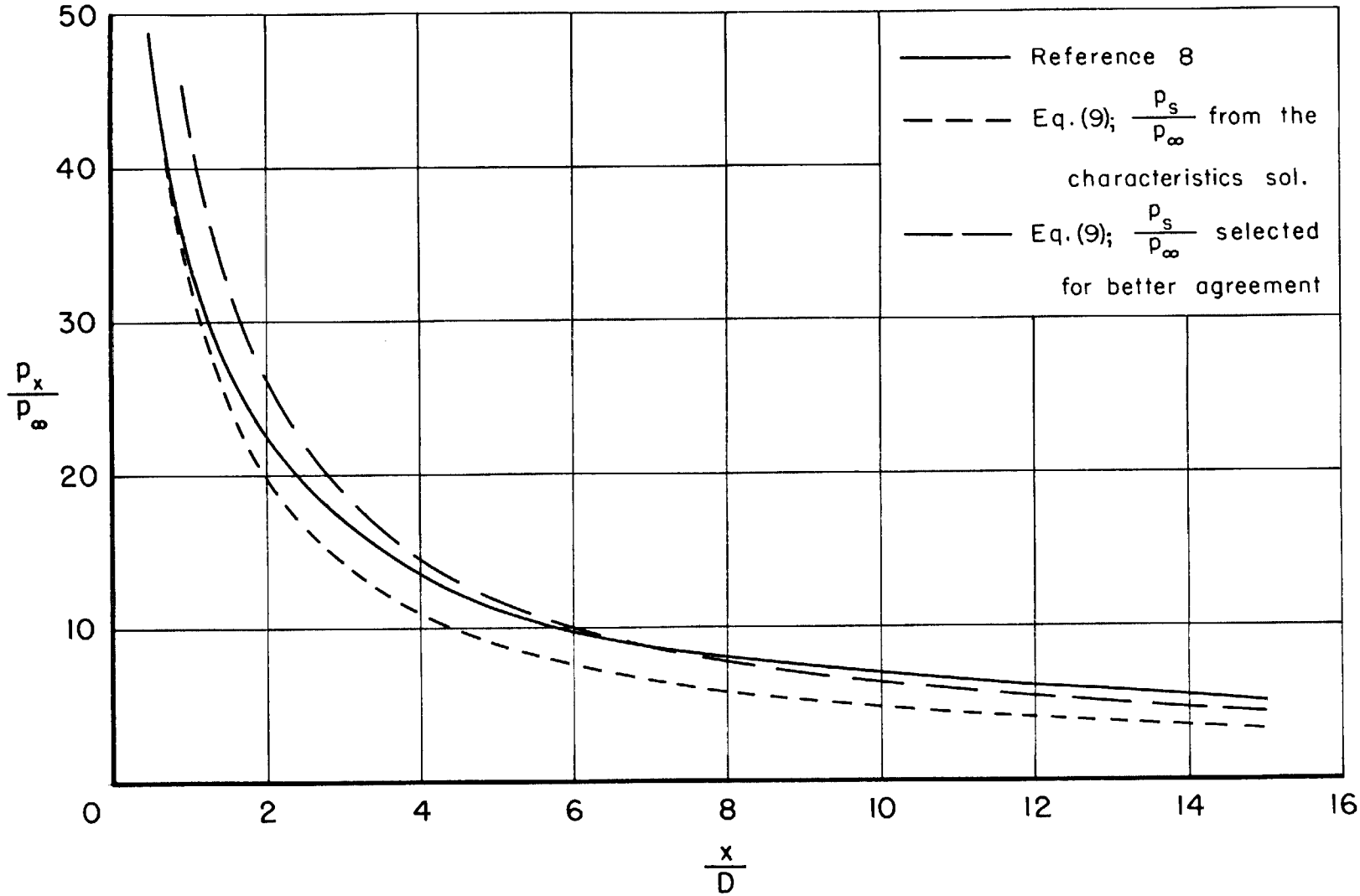

(a) Real air; M_∞ = 35.9, 100,000 feet altitude.

Figure 18.- Comparison of characteristics solutions for a hemisphere-cylinder with the pressure-decay method for selected values of initial pressure.

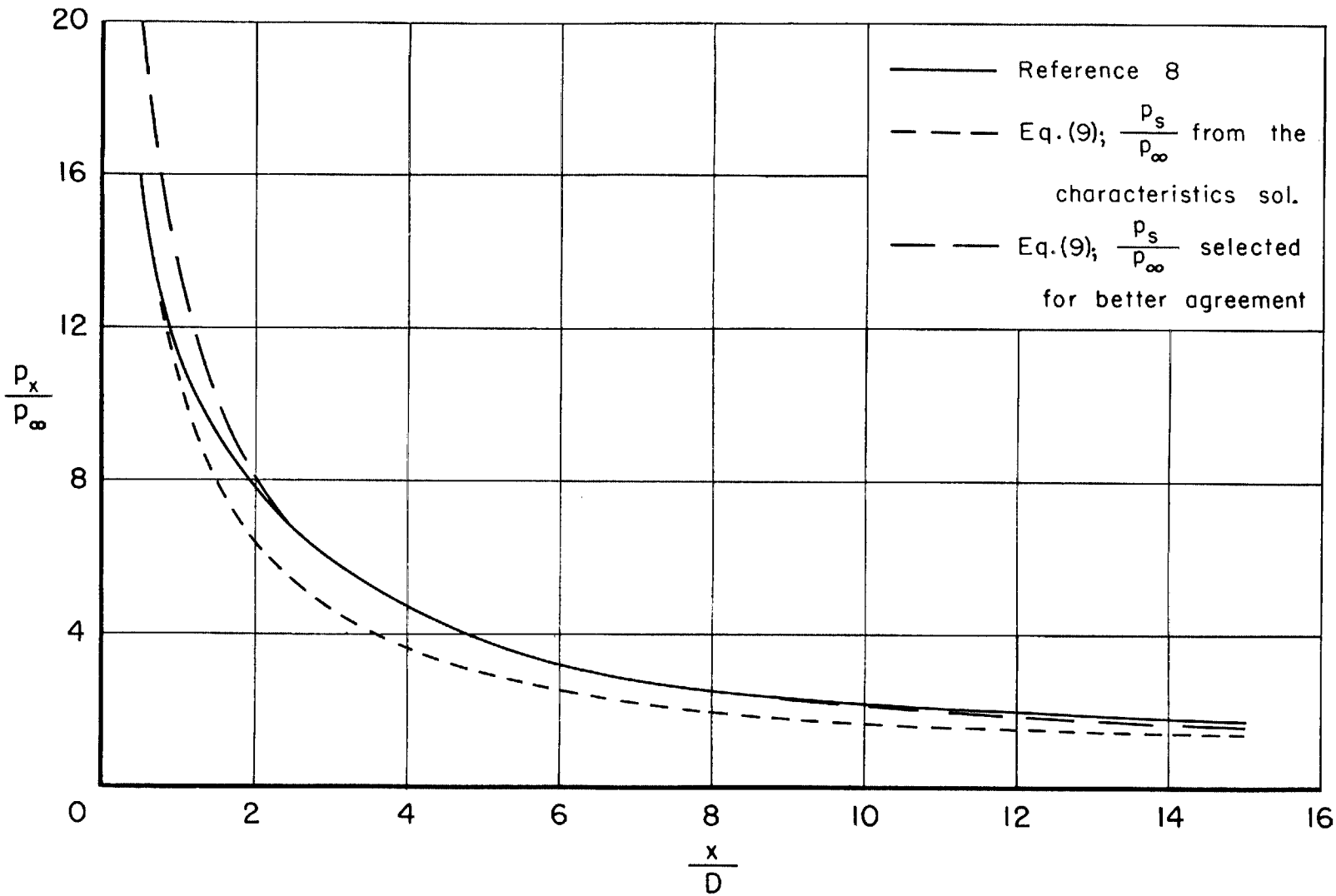

(b) Perfect air; $M_\infty = 18$.

Figure 18.- Concluded.

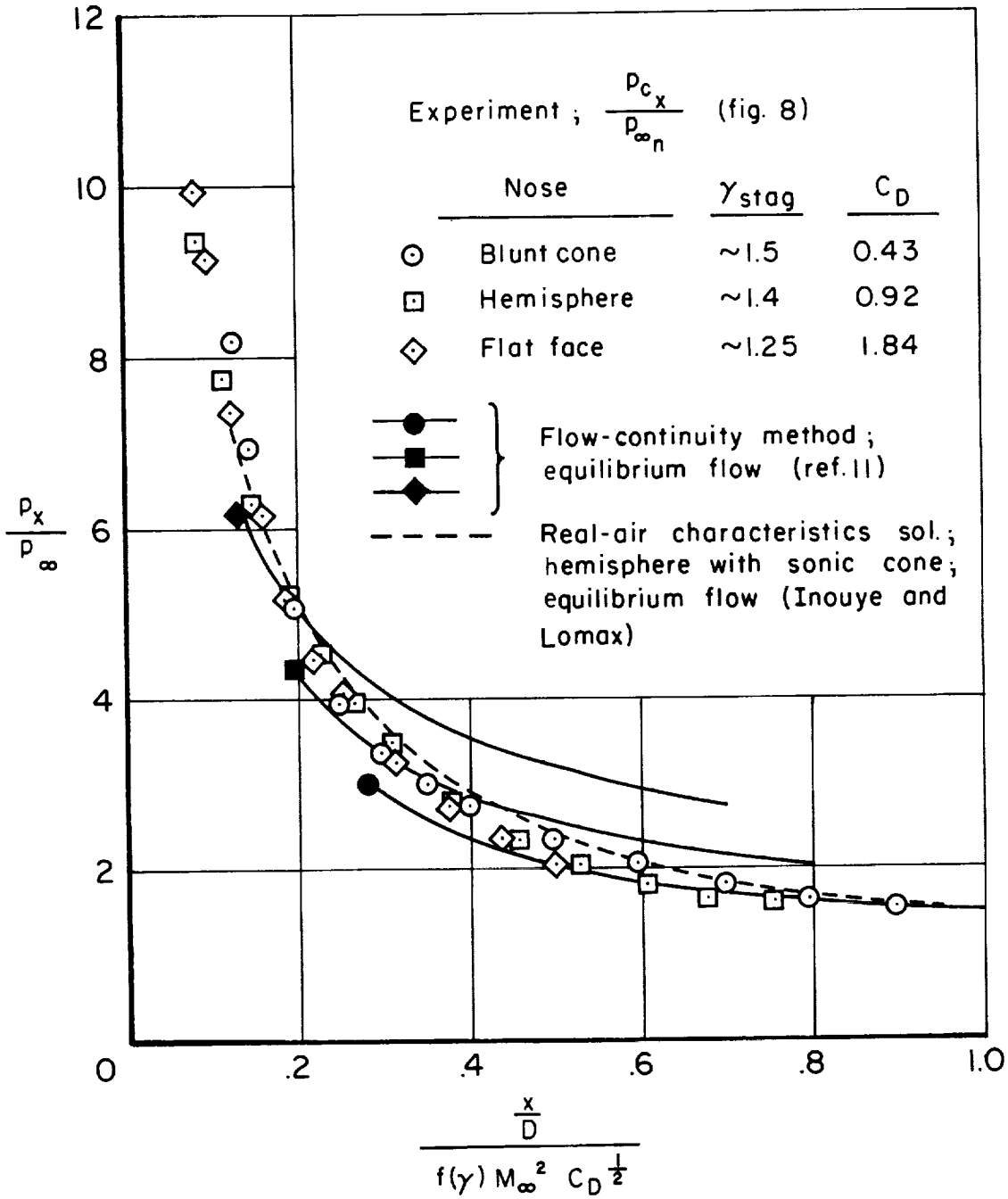

Figure 19.- Experiment compared with real-air characteristics and flow-continuity methods; $M_{\infty_n} = 14.4$.